2011

Simulation study of sweep improvement in heavy oil CO2 floods

Venu Gopal Rao Nagineni
Louisiana State University and Agricultural and Mechanical College

SIMULATION STUDY OF SWEEP IMPROVEMENT IN HEAVY OIL CO_2 FLOODS

A Thesis

Submitted to the Graduate Faculty of the
Louisiana State University and
Agricultural and Mechanical College
in partial fulfillment of the
requirements for the degree of
Master of Science in Petroleum Engineering

in

The Craft and Hawkins Department of Petroleum Engineering

by
Venu Gopal Rao Nagineni
B. Tech., Indian School of Mines, India, 2006
May, 2011

ACKNOWLEDGEMENTS

The author expresses his sincere thanks to Dr. Richard G. Hughes for his guidance, encouragement, patience and enlightenment throughout the course of this work at Louisiana State University. His valuable inputs during this research and while writing the thesis were extremely helpful. He showed me different ways to approach a problem and the need to be persistent in order to accomplish any goal.

Thanks to Dr. Christopher White and Dr. Mileva Radonjic who were supportive of this work and enthusiastic to serve on the examining committee.

Thanks to the U. S. Department of Energy, for funding this project under Award Number DE-FC-26-04NT15536. Thanks to David D'Souza and Joseph Barone for providing the resources needed to complete this thesis, and for providing me the opportunity for summer internship.

Thanks are also extended to all the faculty members and students who have offered help and made the past several years enjoyable and worthwhile.

Lastly, thanks to my parents, sister, brother, cousins and my little nephew Aarav, who inspired and supported me all along.

TABLE OF CONTENTS

LIST OF TABLES

LIST OF FIGURES

ABSTRACT

Enhanced oil recovery by CO_2 injection is a common application used for light oil reservoirs since CO_2 is relatively easily miscible with light oils. CO_2 flooding in heavy oil reservoirs is often uneconomic due to unfavorable mobility ratios. Reservoir heterogeneity further complicates the process as CO_2 channels through high permeability layers leading to premature breakthrough. However, this can be controlled by choosing a suitable modification to the CO_2 injection process enabling better sweep efficiencies, and making the process economic. The current work focuses on two such methods; water-alternating-gas injection (WAG) and profile modification by blocking gas flow in the high permeability layer. These methods were studied for physical mechanisms of oil recovery, increasing sweep efficiency, and mitigating premature breakthrough. Reservoir simulation studies of these methods were conducted using an analog heavy oil (14° API) field with a high permeability streak which had 50 times greater permeability than the adjacent zones. A detailed fluid characterization was performed to accurately represent the reservoir fluid. Slim tube and core flood simulations were interpreted to understand the physical mechanisms of oil recovery for this crude. Profile modification using a blocking agent showed very encouraging results. Different WAG ratios were also evaluated, and a WAG ratio of 1:1 resulted in the highest oil recovery which was consistent between both core flood simulations and field simulations. This is different from WAG ratios for highest recovery in light oil reservoirs where values of 1:2 are typically seen. It is shown that with careful study of the reservoir geology and fluid properties,

application of these methods can significantly improve sweep efficiency and oil recovery in heavy oil floods.

1 INTRODUCTION

1.1 Introduction

Enhanced Oil Recovery (EOR) is widely used to recover more oil from an oil field after its primary production phase. Depending on the characteristics of the crude oil and the reservoir properties, an EOR process is chosen to provide economic incremental recovery. Some of the common EOR techniques include non-thermal methods like waterflooding, gas flooding, chemical flooding, and thermal methods like steam flooding and in-situ combustion.

The American Petroleum Institute defines heavy crudes as those with API gravity between 10.1^{o} and 22.3^{o}, while crude oils with API gravity less than 10.1^{o} are defined as extra heavy crudes and bitumen, and those with API gravity greater than 22.3^{o} are defined as light crudes. When it comes to recovering heavy oils, thermal methods are the most preferred. According to the US-DOE, the US has an estimated 100 billion barrels of heavy oil resource, of which 80 billion comes from 248 large reservoirs mostly in the states of California, Alaska, and Wyoming. The states of Louisiana, Arkansas, Mississippi, and Texas also have significant volumes (DOE, 2007). Nearly 50% of these oil reservoirs do not offer favorable conditions for the application of thermal methods. They may have thin formations, excessive depths, low permeability, high viscosity, and/or low oil saturations. Non-thermal recovery methods like waterflooding and carbon dioxide (CO_2) flooding would best suit these heavy oil reservoirs (Ali, 1976).

The CO_2 flooding process is a very widely used EOR mechanism, employed primarily for light oils during tertiary recovery. In 2006, there were 80 active CO_2 miscible projects and two active CO_2 immiscible projects in as many as nine different states in the US (Worldwide EOR Survey, 2006). CO_2 has several advantages when compared to using other gases for flooding and is often a preferred displacing fluid depending on its availability. Some advantages of using CO_2 as stated by Mungan (1981) are (a) reduction of crude oil viscosity, (b) swelling of crude oil, (c) miscibility effects, (d) increase of injectivity, and (e) internal solution gas drive. However, gravity over-ride, mobility effects, asphaltene deposition, and reservoir heterogeneity might severely affect the performance of a CO_2 flood (Mungan, 1981).

As nations all over the world increase their efforts to reduce emissions of greenhouse gases and sequestering current CO_2 emissions, CO_2 injection into oil reservoirs to recover more oil cannot be overlooked as a method to sequester carbon dioxide. Total US CO_2 emissions in 2007 were 5,991 million metric tons and are expected to increase 0.3 percent per year until 2030 (EIA, March 2009).

1.2 Literature Review

There has been considerable research on CO_2 flooding in heavy and light crudes, and miscible and immiscible processes (Lake, 1989). Heavy oils have a higher concentration of heavier carbon compounds, which makes it difficult to achieve miscibility at normal reservoir

conditions. There have been several laboratory and field studies conducted to evaluate immiscible CO_2 processes in heavy oil systems. Laboratory experiments concentrated on core flood studies with different compositions of crude, variation to the CO_2 flood process, and modifications to the slug size during a flood.

Sweep efficiency for lighter crudes has been extensively studied and literature is dedicated towards extraction of light oils using waterflooding (Craig, 1993) and CO_2 flooding methods (Jarrell, et al., 2002). Furthermore, sweep improvement and conformance control methods for light crudes have been discussed by Martin, et al. (1988) and Syahputra, et al. (2000). The greater mobility difference between CO_2 and heavy oil may result in very low sweep efficiencies; therefore using sweep improvement techniques is one way to improve sweep efficiency and eventual oil recovery. Although the most commonly used methods for extracting heavy crude are thermal processes like steam injection, the field which the subject of this study has easy access to CO_2. As a consequence, the CO_2 is inexpensive if compared to steam injection or hot water.

One of the first laboratory works on CO_2 flooding of heavy oil systems was done by Jha (1986). He conducted a series of CO_2 flooding experiments on Lloydminster reservoir crude with 15° API gravity using different CO_2 flooding schemes, namely continuous CO_2 injection, CO_2 slug process, injection of alternate slugs of CO_2 and water, and simultaneous injection of CO_2 and water. He observed a forty-five fold decrease in viscosity and a 16% increase in the swelling factor for the tested heavy oil-CO_2 system. The study also observed

that a soak period between CO_2 and water injection in a water-alternating-gas (WAG) process improves recovery.

Further work by Rojas and Farouq Ali (1986) studied CO_2 injection in cores from Lloydminster heavy oils to examine a CO_2 flood's applicability in thin reservoirs like the ones in the Lloydminster field. They observed that CO_2 injection and injection of a slug of CO_2 driven by brine were inefficient due to recycling of injected CO_2. WAG processes proved to be more efficient when using a high WAG ratio (ratio of the volume of water injected to the volume of CO_2 injected). This was contrary to simulation studies conducted at the time which pointed towards lower WAG ratios yielding increased recoveries. The authors documented four mechanisms which contribute to increased oil recovery: oil expansion, viscosity reduction, reduction in interfacial tension, and blowdown recovery.

A laboratory investigation conducted by Mangalsingh and Jagai (1996) on heavy crudes from Trinidad emphasized that solubility and diffusion are the fundamental processes in the effectiveness of CO_2 as a recovery agent. They conducted core floods on heavy to light crudes with API gravities varying from 16^o to 29^o. The authors also noted a higher requirement of CO_2 for lighter crudes in comparison to heavier crudes because of the large quantity of methane in these oils. In lighter crudes, CO_2 removes methane before it mixes with oil and changes its properties. CO_2 mixes with oil by diffusion as well as by solution.

Most of the simulation work on immiscible and/or miscible CO_2 flooding is done as part of field studies and hence their focus is on reservoir modeling and evaluating a field

specific optimum WAG ratio (Moffitt and Zomes, 1992; Reid and Robinson, 1981; Hatzignatiou and Lu, 1994; Spivak and Chima, 1984).

Spivak and Chima (1984) conducted 1D, 2D, and 3D simulation studies to investigate mechanisms of immiscible CO_2 injection into heavy oil reservoirs, in particular, two projects implemented in the Wilmington Field, California. The authors stated that the process of immiscible CO_2 drive in heavy oil reservoirs reduces viscosity, followed by waterflooding of the reduced viscosity oil. 1D simulations indicated that CO_2 strips methane from oil and a methane bank is formed just ahead of the injected gas.

Hatzignatiou and Lu (1994) conducted a feasibility study of immiscible CO_2 flooding in the West Sak reservoir in Alaska through simulation. Three different injection processes – continuous CO_2 injection, CO_2 WAG and CO_2 slug injection – were simulated in 5-spot and 9-spot patterns, and their ultimate recoveries were compared to a waterflood. They reported an increase in oil recovery with an increase in CO_2 slug size, but the WAG process showed no significant improvement in oil recovery compared to CO_2 slug process. Continuous CO_2 injection yielded the highest recovery.

1.3 Motivation and Objectives

As stated previously, the field that motivated this study has ready access to inexpensive CO_2. However, the field had problems with early breakthrough of CO_2. This thesis examines these problems and uses reservoir simulation and a production match to

evaluate plausible explanations. Later, different methods are proposed which could mitigate the problems, thereby increasing sweep efficiency. Although the CO_2 flooding process in this field is immiscible, slimtube results show a significant recovery of 65% at operating conditions of 3500 psia. Hence, the microscopic displacement efficiency (E_D) of this process is reasonable, and a good macroscopic sweep efficiency (E_V) would improve the overall process efficiency ($E=E_DE_V$) (Green and Willhite, 1998). This motivated the current study.

Preliminary analysis indicates that heterogeneity is causing most of the problems seen in sweeping heavy oil with this immiscible flood. The study investigates methods to enhance the sweep efficiency and ultimate recovery. Heterogeneity effects are more pronounced in heavier oil systems due to the higher mobility ratio, which is one of the disadvantages of an immiscible CO_2 flood. To understand these aspects, we chose to perform reservoir simulation studies on this heavy oil field. The purpose of these simulation studies was to identify the mechanisms which caused early breakthrough and recommend mitigating techniques. Mitigating techniques we intend to examine are WAG and using a profile modification agent.

2 RESERVOIR FLUID MODEL

2.1 Field History

The current work uses data from a heavy oil formation in the continental US. The formation is divided into an upper zone and a lower zone. CO_2 injection has occurred only in the upper zone, so that is the focus of this study. Table 2.1 provides a list of average reservoir properties, and an isopach map of the field is shown in Figure 2.1. The formation is bound on the eastern edge by a fault which runs northeast-southwest, and is bound on the western edge by an aquifer.

Table 2.1: Average Reservoir Properties of the Field

Depth	8500’
Oil Gravity	14 ^{o}API
GOR	50 scf/STB
B_o	1.05 RB/STB (@ bubble point = 1000 psia)
BHP	3900 psig
BHT	198 ^{o}F
Porosity	26.00%
Water Saturation	39.00%
Permeability	71 mD (from sidewall core study)
Average net pay	35’
Reservoir volume (Acre-ft)	6125
OOIP	7.3 MMBO

The zone started production from Well #1. Later, Well #2 was drilled to determine the oil-water contact. Finally, Well #3 was drilled. Initial mapping indicated that Well #3 would

be at a structurally high position, but after drilling the well the reservoir was remapped with Well #1 structurally high. Apart from these wells, Well #4, Well #5 and Well #6 also produce from this zone.

After nearly nine years of primary oil production with an active water drive as the primary drive mechanism, one of the up-dip wells, the #1 well was converted to a CO_2 injector. Because the wells were not in any pattern, injection was designed to sweep oil from the top of the reservoir towards the strong water drive at the bottom, thereby enabling higher production of oil from the down-dip wells. After one month of CO_2 injection (effectively with 17 days of injection) and 0.74 percent HCPV of gas injected, CO_2 breakthrough occurred in the well nearest to the injector, Well #4. Due to this breakthrough, CO_2 injection was curtailed and later stopped. Nearly 2 years later injection began from another well (Well #2) down-dip in the formation, and is currently the only CO_2 injector in the zone. Figure 2.2 shows the field production rates of oil and water along with the number of active production wells.

The well in which CO_2 broke through (Well #4) had no data for the gas produced, hence, an accurate breakthrough time could not be established. However, the field operator indicated that CO_2 injection into the injection well was stopped shortly after CO_2 breakthrough was observed. Using this injection data the breakthrough time was estimated at one month.

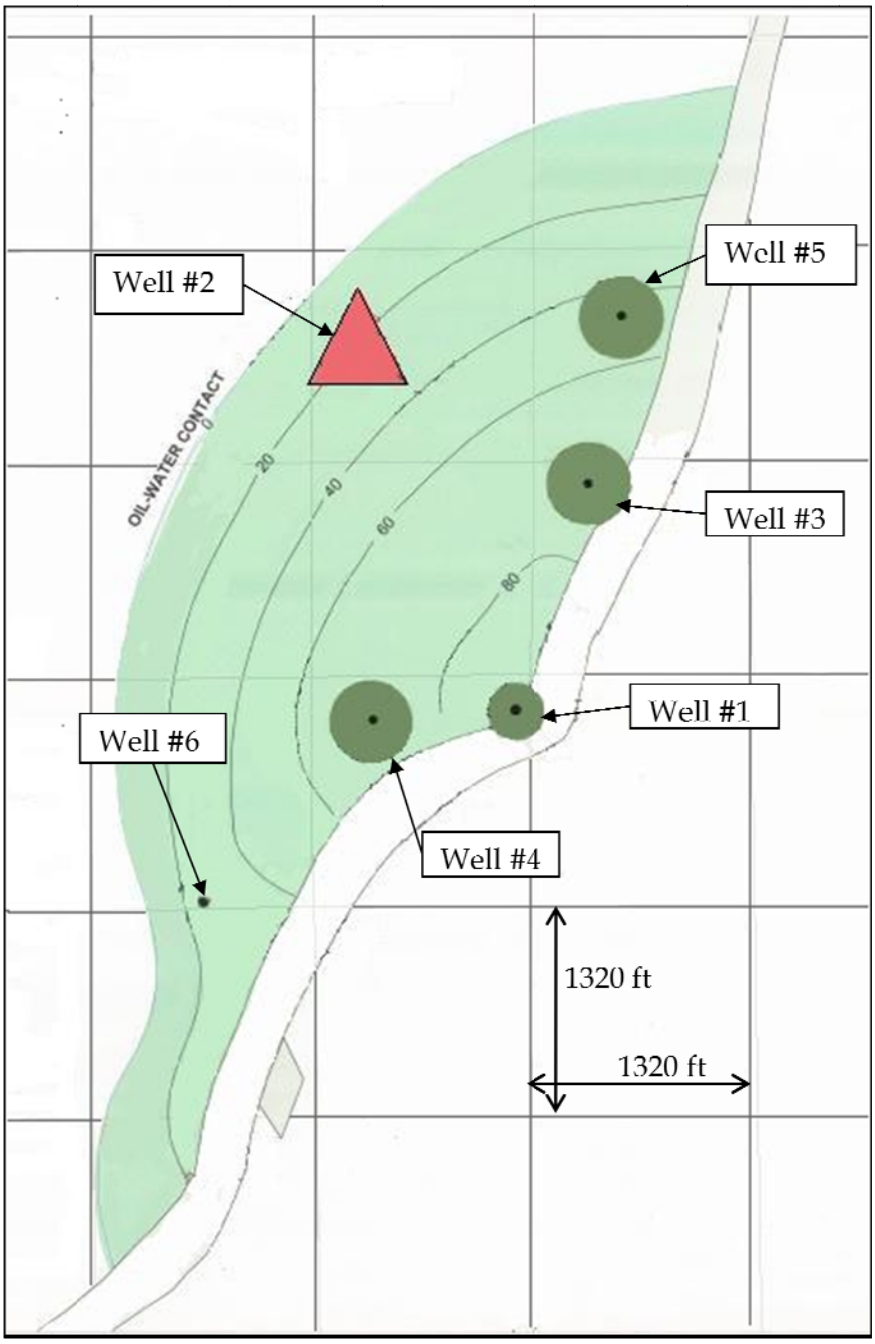

Figure 2.1: Isopach map of the formation of interest. The formation is in an elongated pear shape with a fault on the eastern edge of the formation which runs northeast-southwest. The formation thickness is the maximum (~90 ft) near Well #1. Map shows the current injector (Well #2) as a red triangle. Well #4 saw a premature breakthrough when CO_2 was injected in Well #1.

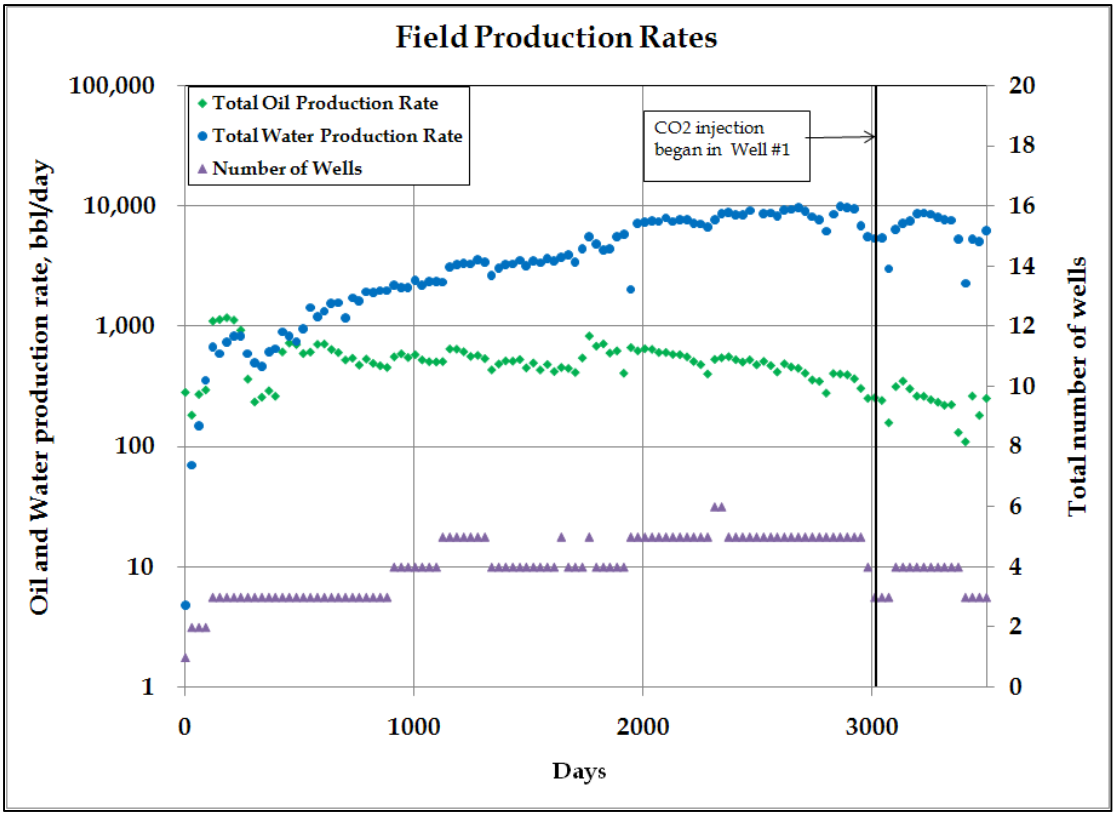

Figure 2.2: Field production rates of oil and water for the field. Water-oil ratio in the field increased gradually due to the presence of a strong aquifer, and reservoir pressure decreased marginally (from material balance calculations) over 9 years of primary production.

2.2 Methodology

A detailed fluid characterization model was built to represent the reservoir fluid in order to study the fluid properties and its effect on the early breakthrough. Next, an analogous 3-D reservoir model was built using the structure & isopach maps, and sidewall core data available from one of the injectors to simulate an approximate history match of the field

production. The model was also used to evaluate mitigation techniques which might increase breakthrough time. A summary of the methodology is:

1. Detailed fluid characterization to capture the fluid properties
    i. Lumping the 40 component system into an 8 component system
    ii. Equation of state tuning using swelling and saturation pressure experimental data
    iii. EOS tuning using experimental viscosity data
    iv. Simulation of slim tube experiments to estimate the minimum miscibility pressure
2. Building an approximate 3D model of the field using data from sidewall cores, and structure and isopach maps.
3. Perform an approximate history match using the field production data to attain reasonably close breakthrough time and productivity behavior.
4. Evaluate early breakthrough mitigating techniques:
    i. Water Alternating Gas (WAG)
    ii. 'Profile modification' techniques such as foam or polymer injection

2.3 Fluid Characterization

The current operator for this field provided fluid composition and component property measurements for the oil and gas from the field. Oxygen free compositional analysis of gas (Table 2.2) and compositional analysis of the stock tank oil (Table 2.3) for the oil and gas produced from Well #4 was provided as performed by the gas chromatography method.

Table 2.2: Oxygen free compositional analysis of As-received gas samples

Cylinder Number	**840250D**	**840263D**	**840279D**	**Mean** (these values were used for gas composition)
Component	**Composition Mol.%**	**Composition Mol.%**	**Composition Mol.%**	
Nitrogen	2.523	2.572	2.562	2.552
Carbon Dioxide	0.078	0.077	0.087	0.081
Hydrogen Sulfide	0.000	0.000	0.000	0.000
Methane	78.085	77.677	78.937	78.233
Ethane	3.228	3.187	3.251	3.222
Propane	3.509	3.447	3.536	3.497
iso-Butane	0.796	0.791	0.805	0.797
n-Butane	2.117	2.113	2.134	2.121
iso-Pentane	1.451	1.515	1.470	1.479
n-Pentane	2.513	2.654	2.514	2.560
Hexanes	3.802	4.185	3.399	3.795
Heptanes	1.723	1.613	1.213	1.516
Octanes	0.175	0.154	0.092	0.140
Nonanes	0.000	0.000	0.000	0.000
Decanes	0.000	0.000	0.000	0.000
Undecanes	0.000	0.000	0.000	0.000
Dodecanes	0.000	0.015	0.000	0.005
Tridecanes plus	0.000	0.000	0.000	0.000
TOTAL	100.000	100.000	100.000	100.000

Table 2.3: Compositional Analysis of as-received Stock Tank Oil

Component		Wt%	Mol%	Molecular Weight gm/mol	Density gm/cc
N_2	Nitrogen	0.000	0.000	28.013	0.809
CO_2	Carbon Dioxide	0.000	0.000	44.010	0.801
H_2S	Hydrogen Sulfide	0.000	0.000	34.080	0.817
C_1	Methane	0.000	0.000	16.043	0.300
C_2	Ethane	0.000	0.000	30.070	0.356
C_3	Propane	0.000	0.000	44.097	0.507
iC_4	iso-Butane	0.000	0.000	58.123	0.563
nC_4	n-Butane	0.001	0.008	58.123	0.584
iC_5	iso-Pentane	0.005	0.033	72.150	0.624
nC_5	n-Pentane	0.011	0.073	72.150	0.631
C_6	Hexanes	0.086	0.489	84	0.685
C_7	Heptanes	0.252	1.268	96	0.722
C_8	Octanes	0.524	2.343	107	0.745
C_9	Nonanes	0.777	3.066	121	0.764
C_{10}	Decanes	1.014	3.613	134	0.778
C_{11}	Undecanes	1.161	3.771	147	0.789
C_{12}	Dodecanes	1.311	3.888	161	0.800
C_{13}	Tridecanes	1.526	4.164	175	0.811
C_{14}	Tetradecanes	1.622	4.076	190	0.822
C_{15}	Pentadecanes	1.768	4.098	206	0.832
C_{16}	Hexadecanes	1.795	3.861	222	0.839
C_{17}	Heptadecanes	1.891	3.810	237	0.847
C_{18}	Octadecanes	1.933	3.677	251	0.852
C_{19}	Nonadecanes	2.062	3.743	263	0.857
C_{20}	Eicosanes	2.005	3.481	275	0.862
C_{21}	Henicosanes	1.962	3.219	291	0.867
C_{22}	Docosanes	1.865	2.920	305	0.872
C_{23}	Tricosanes	1.830	2.748	318	0.877
C_{24}	Tetracosanes	1.802	2.599	331	0.881
C_{25}	Pentacosanes	1.709	2.365	345	0.885
C_{26}	Hexacosanes	1.743	2.318	359	0.889
C_{27}	Heptacosanes	1.754	2.239	374	0.893
C_{28}	Octacosanes	1.727	2.125	388	0.896
C_{29}	Nonacosanes	1.715	2.037	402	0.899
C_{30}	Triacontanes	1.682	1.931	416	0.902
C_{31}	Hentriacontanes	1.595	1.771	430	0.906
C_{32}	Dotriacontanes	1.451	1.560	444	0.909
C_{33}	Tritriacontanes	1.408	1.468	458	0.912
C_{34}	Tetratriacontanes	1.284	1.299	472	0.914
C_{35}	Pentatriacontanes	1.246	1.224	486	0.917
C_{36+}	Hexatriacontanes plus	55.483	18.715	1415	1.063

WINPROP® 2009.10 from the Computer Modeling Group, Ltd (CMG) was used for fluid characterization. WINPROP® is CMG's equation of state (EOS) multiphase equilibrium and properties determination program. WINPROP® features techniques for lumping of components, matching laboratory PVT data through regression, generation of phase diagrams, and compositional grading calculations like swelling and viscosity calculations (Computer Modeling Group Ltd., 2009).

The following steps summarize the process used for the fluid characterization

1. Recombination of oil and gas compositions to form live oil under reservoir conditions.

2. Lumping the 40 component fluid system into a smaller number of pseudo-components. The process of component lumping is done by phase diagram match, in which the phase diagram of the original 40 component system is compared with the phase diagram obtained after lumping into pseudo-components.

3. Several cycles of regression were performed on the pseudo-component properties to match the available swelling factor and viscosity data with the values calculated through the software. After each cycle the phase envelope was compared with the 40 component phase diagram. Regression was stopped after a satisfactory match was found between the experimental PVT data and the calculated PVT values, and also between the phase diagrams.

4. Minimum Miscibility Pressure (MMP) and the displacement drive mechanism (condensing and vaporizing drive) calculated by WINPROP® were verified after each cycle of regression to ensure that the MMP value was close to its value before regression, and the drive mechanism remains the same.

5. In the case of an unsatisfactory match between the phase diagrams or MMP, or for a change in drive mechanism, regression controls were altered within ±5% of the parameter value and regression was continued.

2.3.1 Recombination

Oil and gas compositions from the separator gas and the stock tank oil were used to simulate the recombination to form live oil using WINPROP®'s 'Recombination' option, which results in 40 components and their component properties. This recombination needs to be done at separator conditions. Based on communications with the operator, separator conditions of 50 psia and 60 °F were chosen. A gas-liquid phase diagram was generated for this 40 component system. Table 2.4 gives a detailed account of the mole fractions of each component after recombination. Figure 2.3 shows the phase diagram for the 40 component system.

Table 2.4: Components and component mole fractions after recombination to form live-oil

Component	Mole Fraction (%)	Component	Mole Fraction (%)	Component	Mole Fraction (%)
N_2	0.4577	C_{11}	3.0870	C_{25}	1.936
CO_2	0.0141	C_{12}	3.1827	C_{26}	1.8975
C_1	14.164	C_{13}	3.4087	C_{27}	1.8329
C_2	0.5855	C_{14}	3.3366	C_{28}	1.7395
C_3	0.6365	C_{15}	3.3547	C_{29}	1.6675
iC_4	0.1444	C_{16}	3.1606	C_{30}	1.5807
nC_4	0.3906	C_{17}	3.1189	C_{31}	1.4498
iC_5	0.2902	C_{18}	3.01	C_{32}	1.277
nC_5	0.5156	C_{19}	3.064	C_{33}	1.2017
C_6	1.09	C_{20}	2.8496	C_{34}	1.0634
C_7	1.3505	C_{21}	2.6351	C_{35}	1.002
C_8	1.9497	C_{22}	2.3903	$C_{36}+$	15.32
C_9	2.5099	C_{23}	2.2495		
C_{10}	2.9576	C_{24}	2.1276		

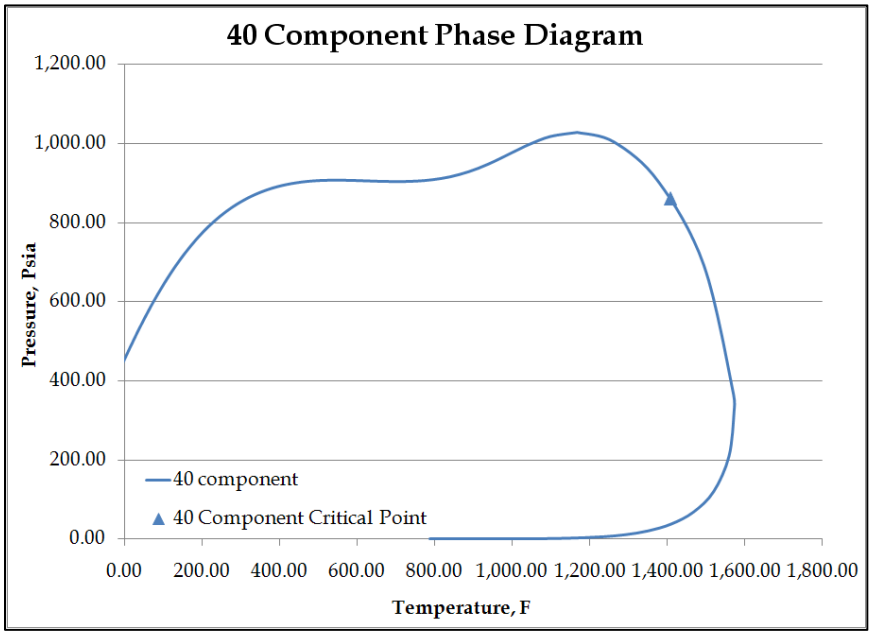

Figure 2.3: 40 component phase diagram.

2.3.2 Lumping of Components

CO_2 injection into a reservoir is a compositional process which alters the components in the crude oil. In compositional simulation, the number of primary equations per grid block is N_c+1, where N_c is the number of components in the hydrocarbon system. Hence, the larger the number of components used, the greater would be the amount of time taken to solve the equations at each time-step. Thus decreasing the number of hydrocarbon components (lumping) would ease the process of simulation (Coats, 1980). However, during the process of lumping care must be taken so that the fluid properties do not change too much in comparison with the original (un-lumped) fluid properties.

A lumping scheme described by Hong (1982) was used to group the 40 component system into an 8 component one. As suggested by Hong (1982), non-hydrocarbon components (CO_2 and N_2) were kept separate, light hydrocarbon compounds (C_1-C_5) were grouped together, and heavier hydrocarbon compounds (C_6-C_{36}^+) were also grouped together. Hong (1982) suggests grouping all components above C_7 into one pseudo-component. However, since the crude oil used in this study has many heavier fractions with relatively large mole fractions, three pseudo-components were formed by grouping together components between C_6 and C_{36}^+.

The lumping scheme described above was developed after several trial runs with different combinations of groupings. Based on the guidelines provided by Hong (1982) a few combinations of groupings were made, and a P-T phase diagram was plotted for each of these

combinations. A lumping combination which provided a good match with the 40 component phase diagram was chosen and used as the lumping scheme. This scheme is shown in Figure 2.4. It shows a good match between the 40 component and 8 pseudo-component lumping schemes. The phase envelope has a near perfect match at reservoir temperature (198° F). Table 2.5 shows the lumping scheme (8 pseudo-components) for which the best match was observed. The heavier fraction, C36+, has a substantial mole fraction of more than 15 percent.

Table 2.5: Lumping and mole fraction of the 8-component system. The heaviest component, C36+, has a substantial mole fraction of 15 percent.

Pseudo-Component	Mole Fraction (%)
N_2	0.4577
CO_2	0.01414
C_1	14.1641
$C_2 - C_3$	1.2220
$C_4 - C_5$	1.3408
$C_6 - C_{12}$	16.1274
$C_{13} - C_{35}$	51.3537
C_{36}^+	15.3202

Figure 2.4 shows the P-T phase diagrams for the 40 and the eight pseudo-component systems along with the 10%, 30% and 50% gas fraction lines. The discontinuity in the gas fraction lines is due to the instability of the Gibbs free energy surface, hence a sudden shift in the phase plot is observed (Computer Modeling Group Ltd., 2009). It can be noted that the instability is always at a temperature greater than the reservoir temperature (198 °F).

Therefore, for non-thermal processes (like CO_2 flooding) this instability does not greatly impact the usable portion of the phase diagram.

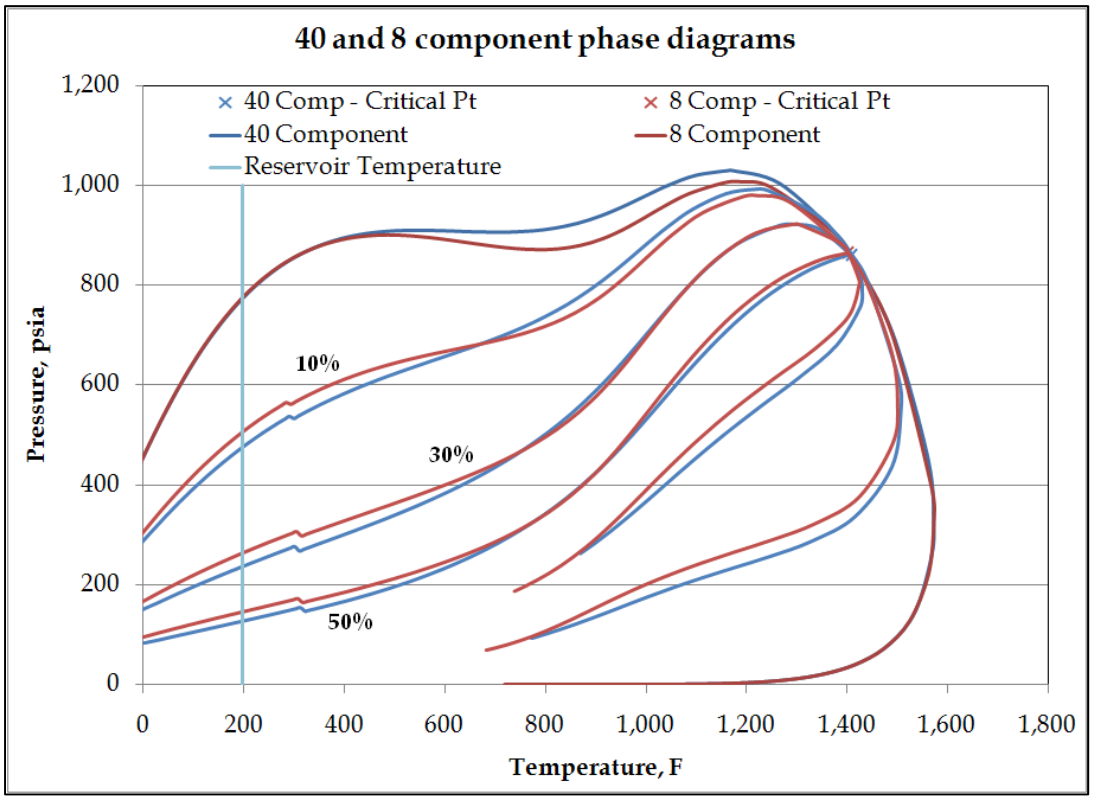

Figure 2.4: Phase diagrams with the 40 component and 8 pseudo-component system. 10%, 30% and 50% gas quality lines are shown in the graph. The discontinuities observed in gas quality lines are above the temperature range of the reservoir under study.

2.3.3 Equation of State Tuning for Swelling and Viscosity Data

The Peng-Robinson equation of state (EOS) was used in this study for fluid modeling. By tuning the EOS parameters, a match can be obtained for the experimental data and thereby

increase confidence in the predictions from the reservoir simulator. Properties of the pseudo-component like, molecular weight, critical pressure, critical temperature, binary interaction coefficients, and Pedersen viscosity coefficients (Pedersen, et al., 1984) were regressed upon in order to match the experimental data. EOS tuning was done based on the experimental data available from two different PVT tests, (a) swelling test, and (b) viscosity test.

2.3.3.1 Swelling and Viscosity Data

After the 40 component system was lumped together to get an 8 pseudo-component fluid system, this was tested against the swelling and viscosity reduction tests using the software in order to match the experimental data provided for these tests.

For the viscosity tests, regression was performed over five Pedersen viscosity coefficients (b_1, b_2, b_3, b_4 and b_5) – while the other parameters were kept constant as suggested in the software manual. For the swelling tests, the Pedersen coefficients were kept constant and regression was performed on pseudo-component properties which affect swelling behavior such as molecular weight (M), critical pressure (P_c), critical temperature (T_c), critical volume (V_c), accentric factor (ω) and binary interaction coefficients (δ). Of the eight pseudo-components, three are ungrouped (CO_2, N_2, and C_1), hence the properties of these three components were not used as regression parameters.

After each cycle of regression run, which consists of a regression run for the swelling test and then a regression run for the viscosity test, the phase diagram was constructed to

compare it with the 40 component phase diagram. After each regression run, the change in value of each regression parameter was verified with its value before regression. If the difference was too large, then the variable bounds of that parameter were decreased to ±5% and regression was carried out again. This was done because the phase diagram before regression (8 pseudo-component phase diagram) had a very good match with the 40 component phase diagram, implying that the EOS parameters are also approximately close to what they ought to be. Any major change in these pseudo-component properties would result in the phase diagrams going out of match.

Figure 2.5 shows the match between experimental swelling data and the calculated swelling values obtained after regression was performed to tune EOS parameters. 'Initial Psat' and 'Initial S. F.' represent the Saturation Pressures and Swelling Factors before EOS tuning. Similarly, 'Final Psat' and 'Final S. F.' represent the Saturation Pressures and Swelling Factors after EOS tuning. In Figure 2.5 regression stops at the fourth data point as the saturation pressure of the fluid is close to the critical point (Computer Modeling Group Ltd., 2009). A good match was obtained between the experimental and calculated data. Figure 2.6 shows the viscosity data match between the experimental data and the simulated values. A very good match was obtained for different mole fractions of CO_2. Also, the magnitude of viscosity decrease is high (25 times) which helps in mobilizing oil and greater recoveries.

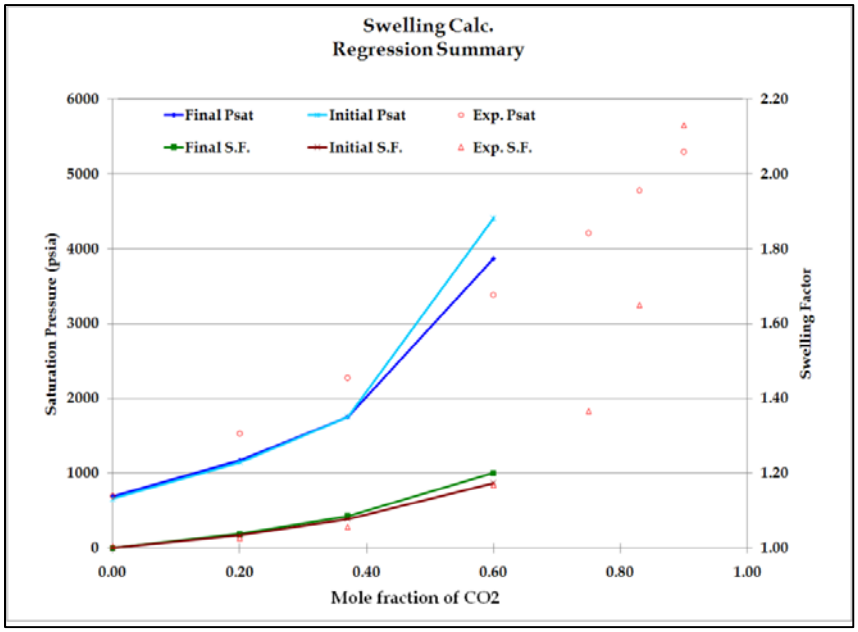

Figure 2.5: Swelling data match after EOS tuning.

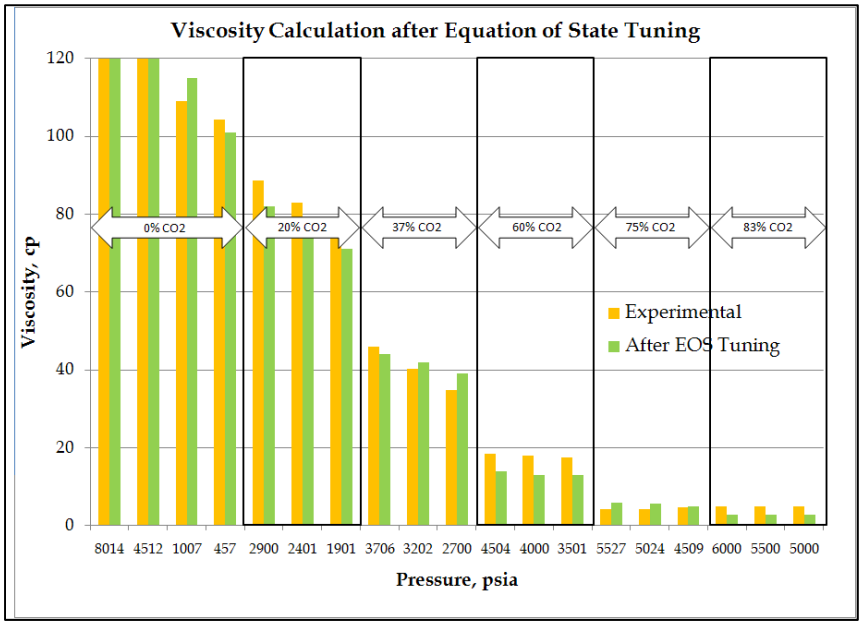

Figure 2.6: Match of EOS tuned viscosity data with experimental viscosity data. CO_2 decreases the oil viscosity 25-30 times.

2.3.4 Slim Tube Simulation

Minimum miscibility pressure (MMP) is an important parameter in miscible displacement processes. MMP is the minimum pressure at which in-situ miscibility can be achieved in a multi-contact miscibility process for a specified fluid system - in this case, CO_2 and the subject crude oil (Green and Willhite, 1998). Slim tube experiments, slim tube simulation, analytical tie-line methods and the vanishing interfacial-tension method are some of the methods used to determine or estimate MMP. In experimental slim tube determination of MMP, it is typically assumed to be the pressure at which there is a 'break' in the curve on a graph of recovery vs. pressure. Thus, it is the pressure above which very little additional recovery occurs (Green and Willhite, 1998).

Slim tube simulation runs were conducted to establish a value for the minimum miscibility pressure. CO_2 flooding processes are not first contact miscible with most crude oils at reservoir conditions and the miscibility process is very often analogous to a vaporizing-gas displacement process (Green and Willhite, 1998).

Slim tube simulation runs were conducted to establish a value for the minimum miscibility pressure using GEM®. GEM® is CMG's advanced equation-of-state compositional simulator which includes various equation-of-state options to simulate CO_2, miscible gases, volatile oil, gas condensate and many other processes that have complex phase behavior and many more (Computer Modeling Group Ltd., 2009). GEM® is used to simulate compositional effects of reservoir fluids during primary and enhanced oil recovery processes. In this work,

the software was used to simulate the impact of CO_2 injection, and to study the effects of the WAG process in mitigating early breakthrough.

For slim tube simulations, a 1D simulation model was constructed consisting of 292×1×1 grid cells of which 290 were 0.2 inch in length and the two grids cells at the either end of the slim tube model were 1 foot in length. The cross-section of the slim tube was ¼ inch by ¼ inch. CO_2 was injected at a low constant rate of 0.0001 bbl/day (0.011 cc/min) into the simulation model and production at the other end was controlled by a minimum bottom hole pressure constraint. The bottomhole pressure was varied for each run from 3500 psia to 9000 psia, in increments of 500 psia. Initial slim tube simulation runs showed a low oil recovery factor of around 70 percent even at higher pressures, owing to a pseudo-component (C_{13}-C_{35}) being largely unswept by the injected CO_2. A 25 percent mole fraction of this pseudo-component was unswept from the oil phase. This was attributed to the binary interaction coefficient between CO_2 and the C_{13}-C_{35} pseudo-component. Hence, after consulting CMG personnel, that particular binary interaction coefficient was changed to 0.094, from 0.3689, which was obtained after EOS tuning. It was also noted that this change in interaction coefficient does not cause major changes in the phase diagram, and it was very similar to the one presented in Figure 2.4.

Table 2.6 shows the values for the interaction coefficients between the pseudo-components from the matching.

This interaction coefficient table was used in all further slim tube simulations and later, in the simulation of sweep improvement methods. A graph of the oil recovery factor

after injecting 1.2 Hydrocarbon Pore Volumes (HCPV) of CO_2 versus the pressure in the slimtube model (Green and Willhite, 1998) is shown in Figure 2.7. This figure shows an increase in oil recovery with pressure until 8500 psia, and flattens after 8500 psia, which shows that the MMP is between 8000 psia and 8500 psia. The MMP value calculated through WINPROP® was 8550 which is in general agreement with the value obtained in the slim tube simulations. WINPROP® uses an analytical tie-line method to calculate MMP by constructing a pseudo-ternary diagram (Computer Modeling Group Ltd., 2009). Moreover, WINPROP® reported a condensing drive as the mechanism by which miscibility was achieved (Computer Modeling Group Ltd., 2009), which is normally the drive mechanism for heavy oil crudes (Green and Willhite, 1998).

The fluid model and the EOS parameters obtained through regression analysis of experimental data were used in further reservoir simulation studies. However, after constructing the fluid model, the operator provided us with PVT data which consisted of a Constant Composition Expansion (CCE) test. The fluid model presented above gave a satisfactory match to the PVT data obtained from the CCE experiments. These plots are shown in APPENDIX A.

2.3.5 Mechanism of Recovery

The above slimtube simulations were studied in order to understand the mechanism of recovery and which components were stripped by CO_2 from the oil phase. CO_2 flooding in slim tube simulations was found to form a bank of lighter oil fractions (C_1, C_2 and C_3) ahead

of the front. Intermediately heavy and heavy fractions do not show this behavior. Figure 2.8 shows the decrease in oil viscosity across the CO_2 front. The plot shows the normalized mole fractions of each of the pseudo-components in the produced fluid. Normalized mole fractions are calculated by taking a ratio of the instantaneous mole fraction of a pseudo-component in the produced fluid and the mole fraction of the pseudo-component before beginning the flood. This behavior has also been reported in many previous studies (Green and Willhite, 1998; Klins and Ali, 1982; Lake, 1989).

Table 2.6: Interaction coefficients between the 8 pseudo-components. The interaction coefficient between CO_2 and C_{13}-C_{35} was changed from 0.3689 to 0.094

	N_2	CO_2	C_1	C_2-C_3	iC_4-nC_5	C_6-C_{12}	C_{13}-C_{35}	C_{36}^+
N_2								
CO_2	-0.41029							
C_1	0.40000	0.15669						
C_2-C_3	0.06752	0.47396	0.00181					
iC_4-nC_5	0.09500	0.59268	0.00050	0.00419				
C_6-C_{12}	0.01290	0.69285	0.09294	0.11724	0.08110			
C_{13}-C_{35}	0.00	0.094	0.10585	0.13122	0.09337	0.00053		
C_{36}^+	0.00	0.00	0.10657	0.13200	0.09406	0.00059	0.0000015	

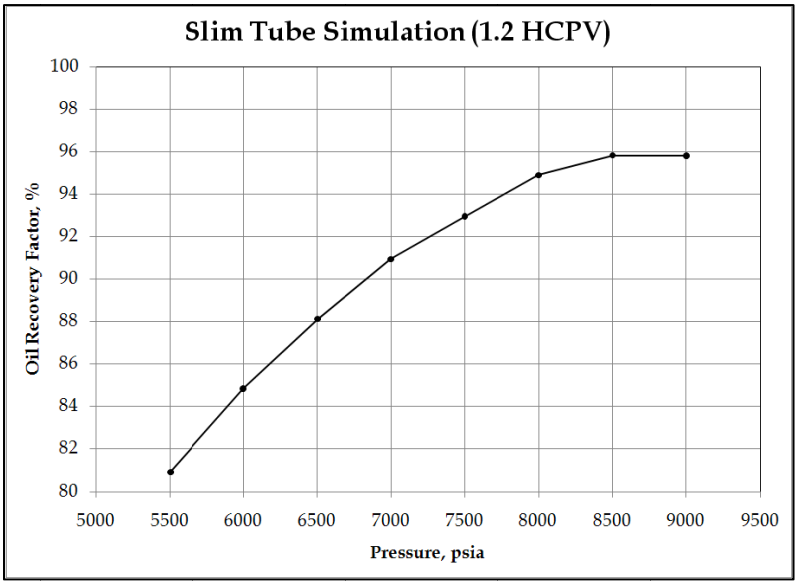

Figure 2.7: Slim tube simulation results estimate an MMP between 8000 psia and 8500 psia.

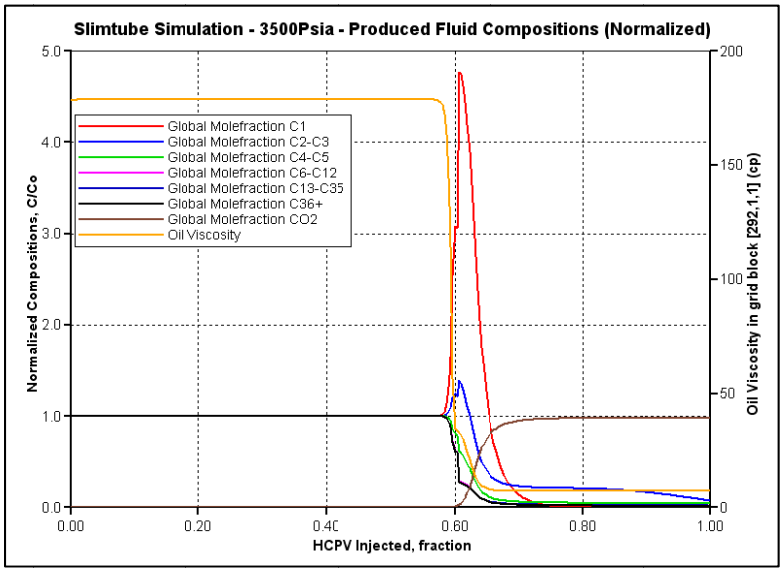

Figure 2.8: Normalized mole fractions of pseudo-components in the produced fluid. Normalized mole fractions of lighter fractions (C_1 and C_2-C_3) increase ahead of the front indicating the formation of bank of lighter components ahead of the front. Also oil viscosity decreases from 180 cp to around 7 cp which is almost a 25 fold decrease.

3 MODEL DESCRIPTION

3.1 Reservoir Model

The target reservoir is small with an estimated original oil in place (OOIP) of 7.34 MMSTB. This reservoir has a strong water drive mechanism which has helped maintain pressure during the nearly 9 year primary production phase. During this period approximately 1.61 MMSTB was produced.

3.1.1 Material Balance Calculation

Reservoir pressure data was not readily available in this field. To get an estimate of the average reservoir pressure at the time CO_2 injection began, a material balance calculation, (Equation 3.1) was done and an average reservoir pressure of 3650 psia was predicted. This suggests a very small drop in reservoir pressure of around 250 psia, over a period of more than 8 years, further confirming the presence of a strong aquifer drive. Material balance also pointed towards a large quantity of water encroachment into the reservoir of 13.9 MMbbls. Cumulative water produced during this period was 12.3 MMbbls.

Table 3.1 provides a list of properties used in the material balance equation. Initial fluid properties were obtained from the operator's well files. Formation (C_f) and water (C_w) compressibilities were not found in any files, and hence were assumed. Fluid properties after

primary production were generated using an MS-Excel® PVT properties Add-In which uses correlations for fluid properties available in literature (McMullan, 2001).

$$\Delta P = \left[\frac{N_p \left[B_o + \left(R_p - R_{so} \right) B_g \right] + W_p B_w - W_e}{N} - \left(B_t - B_{ti} \right) \right] \left[\frac{1}{B_{oi} \left(\frac{C_f + C_w S_{wc}}{1 - S_{wc}} \right)} \right]$$

Equation 3.1

After primary production the reservoir was assumed to be at a pressure, P. Fluid properties were generated at this pressure and were used in Equation 3.1 to calculate ΔP. If the sum of P and ΔP does not equate to 3900 psi, then the P value was suitably changed and the process was continued until convergence. This process yields a reservoir pressure of 3650 psi at the end of primary production.

3.1.2 Sidewall Core Study

Percussion sidewall cores were taken from two of the wells in the field; Well #1 and Well #3. This data was then used to build a simplified geologic model for this work. Sidewall cores taken from the #1 well showed an arithmetic mean porosity of 21.2% and an arithmetic mean permeability of 33 mD (log mean permeability was 12.4 mD). The maximum and minimum permeability for this well from the sidewall cores were 154 mD and 0.93 mD, respectively.

Table 3.1: Initial and final fluid properties used in material balance equation. Fluid properties after primary production were generated through correlations.

Initial Properties		After primary production	
Pressure, psi	3900	Pressure, psi	3658
Temp, F	198	Np, stb	1,611,254
API	15	Gp*, Mcf	44,436
Sep P, psi	50	Wp, bbl	12,677,284
Sep T, F	60	Rp, scf/stb	27.57
GOR, SCF/STB	50	Bo, rb/stb	1.07
Gas Gravity	0.8	z	0.86
Boi, rb/stb	1.05	Bg, rb/scf	0.000776
Bti, rb/stb	1.05	Rs, scf/stb	402.98
C_f, microsips	25	Bt, rb/stb	1.09
C_w, microsips	10	Bw	1.03
*- Gas production data was not available from all the wells			

3.1.3 Modified Lorenz Plot

A modified Lorenz (ML) plot (Nagineni, et al., 2011) was constructed using the sidewall core data for Well #1. A ML plot is a modified version of the Lorenz plot which is a cross plot of cumulative storativity ($\phi \times h$) and cumulative flow capacity ($k \times h$). It is typically used to define flow units within a stratified reservoir. In a Lorenz Plot, the cumulative flow capacity and cumulative storage capacity are ordered from smallest to largest. In a ML plot, cumulative flow capacity and cumulative storage capacity are plotted in the stratigraphic order in which they are found, starting from the base of the reservoir. Assuming there are enough data points to work with and the measurements are representative of the formation being evaluated, data points corresponding to a high slope (greater than 45°) on a ML plot represent sections of the reservoir with high flow capacity but low storage capacity. Low slope regions indicate zones of lower flow capacity and higher storage capacity. Sections

having a slope of 45° represent zones which have a similar average k/ϕ ratio. Each of these constant slope sections can be defined as flow unit intervals within the reservoir (Gunter, et al., 1997). Figure 3.1 shows the Modified Lorenz plot constructed using the sidewall core data from Well #1. It can be noted that the ML plot has a region with a pronounced high slope, which is stratigraphically equivalent to a 16' interval near the center of the formation. This zone is a high permeability streak which accelerates fluid flow and could be one of the main causes for the observed fast breakthrough.

A cross plot of the porosity and permeability values from the sidewall cores in this well shows a very good correlation with a correlation coefficient of 0.9886 (Figure 3.2). In order to tie the measured sidewall core data from Well #1 with its well log information, neutron and density porosity logs were shale corrected to calculate the effective porosity, which was later used to compare with the sidewall core data (Figure 3.3). Two different shale corrected porosities are shown in the figure, one using the Gamma Ray log and the other using the Resistivity log. The four data points shown in square shape correspond to the four data points which follow a very high slope on the ML plot. A large number of sidewall cores which had permeability lower than 20% did not correlate with the log porosity.

Sidewall core data from Well #3 was used to construct a ML plot, but it did not show the high slope section similar to the one found in Well #1. The data points are very close to the homogenous line as shown in Figure 3.4, indicating that the rock formation around this well is homogenous. From these two ML plots, it appears that the reservoir has a few high permeability streaks, and these streaks are local to certain parts of the reservoir. Since, a clear

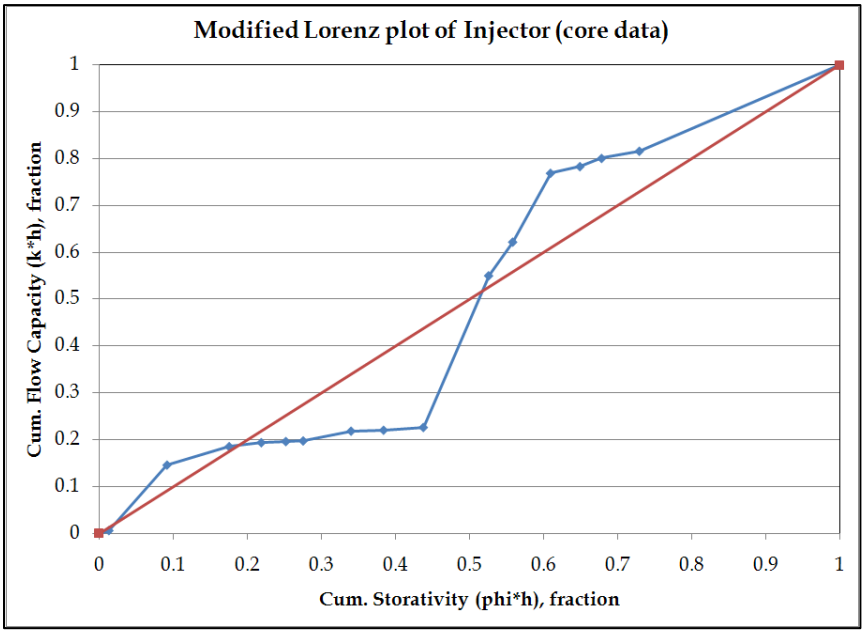

Figure 3.1: Modified Lorenz plot of the Injector well (Well #1). The high slope section in the plot corresponds to a high flow capacity zone from which CO_2 can channel and breakthrough in the production well.

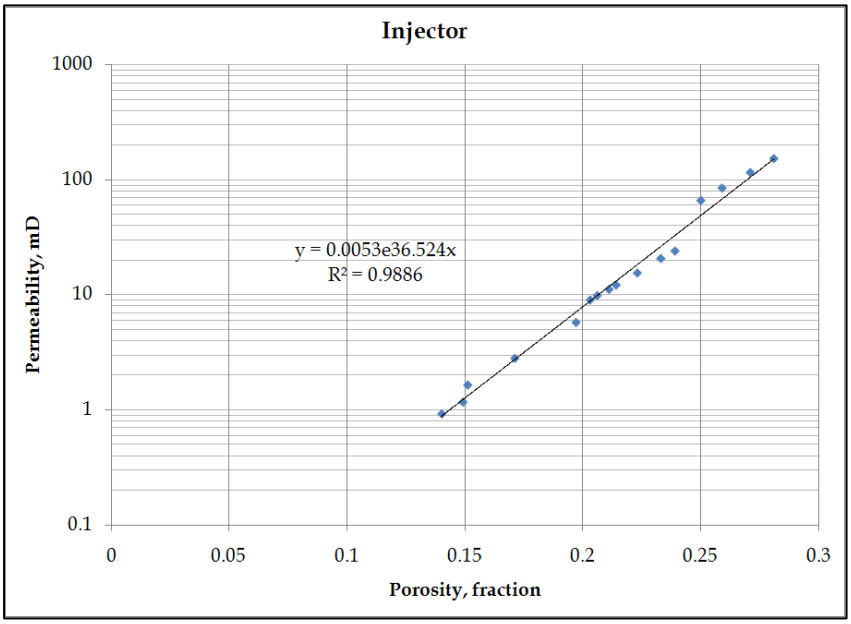

Figure 3.2: Cross plot of porosity and permeability for Injector well (Well #1)

demarcation of the extent of these high permeability streaks could not be made, a global high permeability streak with an aerial extent throughout the field was used to construct the reservoir model. This was viewed as an extreme case to test early breakthrough mitigation techniques. Porosities and permeabilities from the sidewall core data of the injector well were used in the initial reservoir model.

3.1.4 Construction of Reservoir Model

The structure and net pay isopach maps were digitized using WINDIG 2.5 (Lovy, 1996). These digitized maps were imported into CMG Builder® to begin the process of building the model. A three dimensional Cartesian grid system with 50×80×5 was constructed using the maximum number of cells allowed by the University's license (20,000 grid cells). Grid dimensions in both the X and Y direction were 100 ft. The grid dimensions in the Z direction were divided equally between the 5 layers and varied depending on the thickness of the sand. Grid blocks which did not lie within the bounds of the structure map were set to NULL, which assigns zero porosity to the block (Computer Modeling Group Ltd., 2009).

The target sand is believed to have a strong aquifer. A Carter-Tracy infinite aquifer model was selected to represent the water influx from the aquifer, and the aquifer was connected structurally beneath the reservoir sand. Aquifer parameters like porosity, permeability, aquifer thickness, and aquifer radius were adjusted during the course of the history matching process.

Sidewall core data was used to assign the values of permeability in the five vertical layers. A porosity of 25 percent was used for all the layers and permeability values of 10, 10, 135, 25, and 25 mD were used for each layer, starting from the top layer. The third layer had the highest permeability, acting as the high permeability streak.

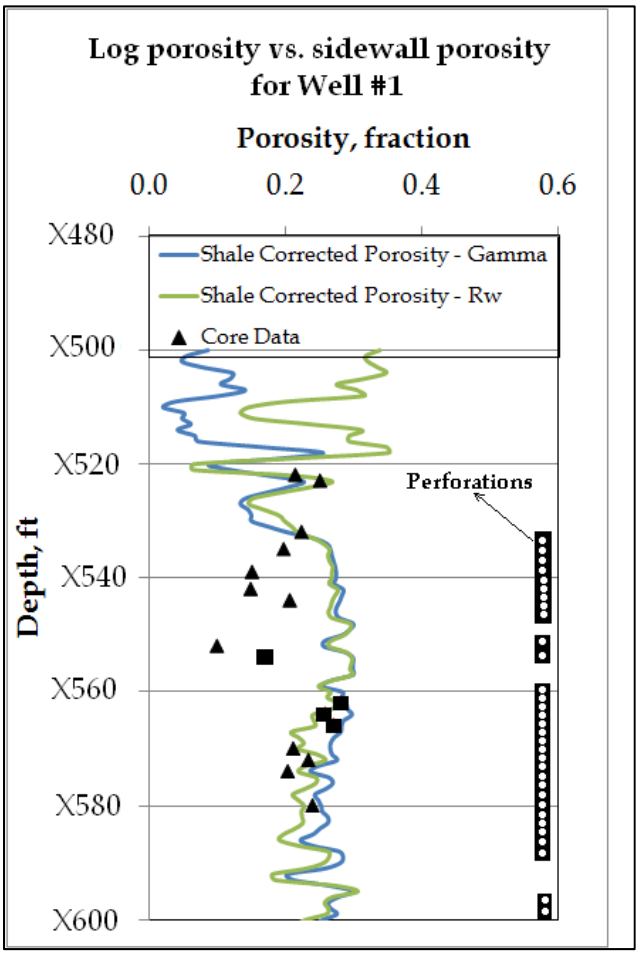

Figure 3.3: Comparison of log porosity vs. sidewall porosity in injector well (Well #1). Zone of interest is X520'-X610'. Perforation intervals are shown in the figure on the right side. Data points shown in square shape correspond to the sidewall core data which show a high slope in the ML plot.

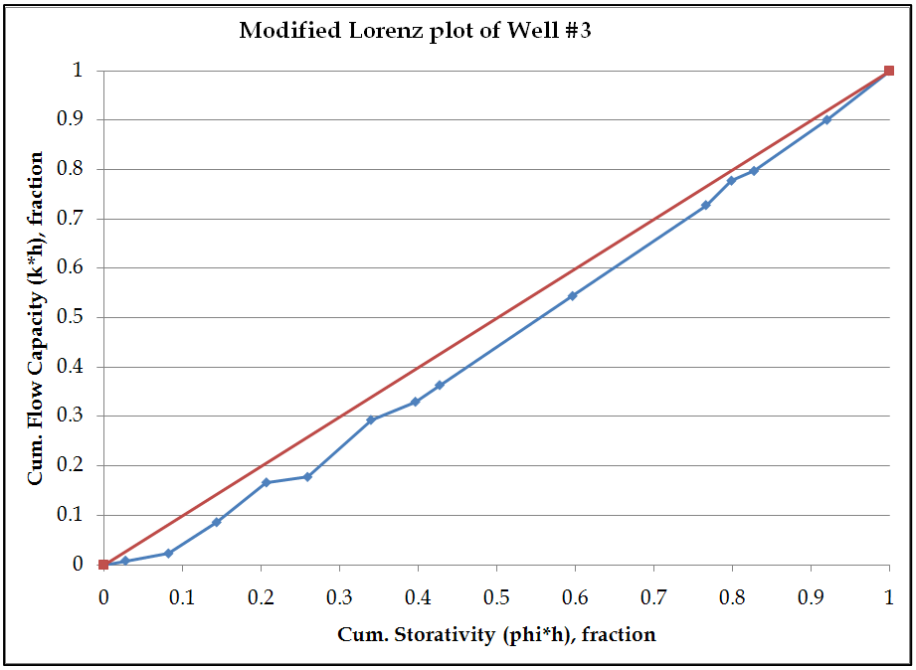

Figure 3.4: Modified Lorenz plot of Well #3. The sidewall core data from this well is parallel to the homogeneous line, representing a homogenous (uniform k/ϕ) formation.

3.2 History Match

Simulation runs to "history match" the reservoir's pre-CO_2 flood oil and water production during primary depletion, were run using the reservoir model described above. During the history match period oil production rates were used as primary constraints, and bottomhole pressures were used as the secondary constraints. After several simulation runs, and with changes made to aquifer properties, relative permeability table, and well productivity indices, the oil rates were below the actual production rates (Figure 3.5). During the simulation runs it was observed that the simulator switched to the secondary constraint since

the production rates (primary constraint) were not met. Modifications had to be made to the reservoir properties to increase the simulated oil rates. Two options which were studied were,

1. Multiplying the permeability of the whole reservoir by a certain factor, and

2. Increasing the permeability of the high permeability third layer.

Both these options gave good history matches. Figure 3.6 shows the field history match of oil production when the model permeability values were multiplied by 5. Figure 3.7 shows the field history match of oil production when the permeability of the third layer was increased from 135 mD to 1 Darcy. The second option was retained as a modification to the existing reservoir model since it encapsulates the high permeability streak, and would allow testing of sweep mitigation techniques in a layered system.

History matching was done in order to get a reasonably close match to field water production rates, and simulations showed a good history match with the water production data. Figure 3.8 shows the history match of water production from the reservoir. After history matching, the reservoir model will be at approximately the same pressure and saturation conditions just prior to when CO_2 injection began.

APPENDIX B shows the production history match plots for individual wells and a description of the observed trends.

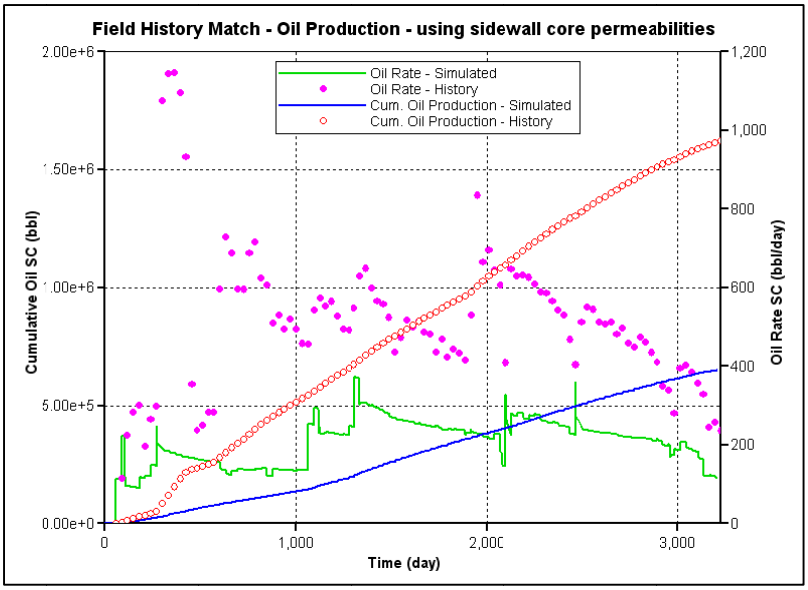

Figure 3.5: History match of oil production rate using the sidewall core permeabilities in the reservoir model. The simulated production rates are lower than the field rates due to the small permeabilities used in the model.

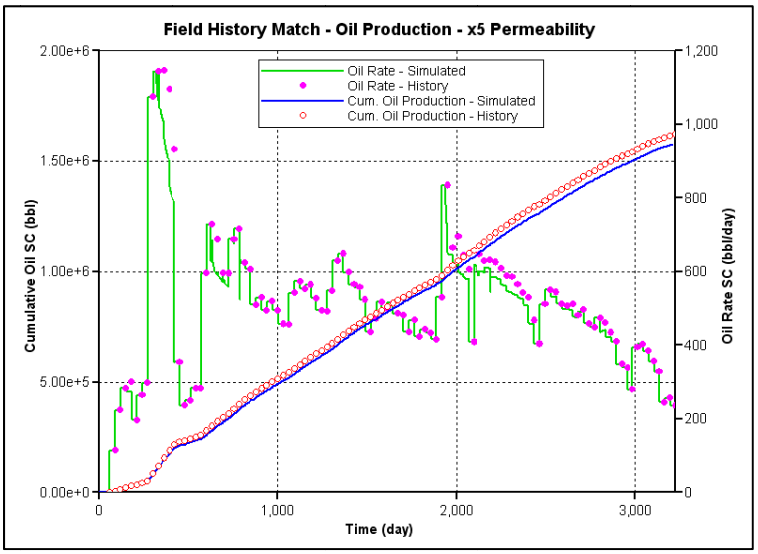

Figure 3.6: Field history match using five times the sidewall core permeabilities.

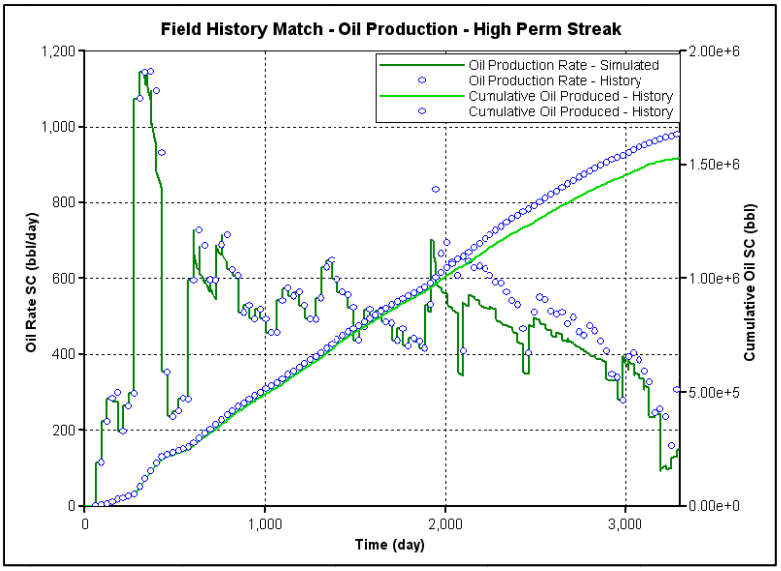

Figure 3.7: Field history match of oil production using 1 Darcy as the permeability of the third layer (high permeability streak). After 2000 days, the simulator switches from the primary constraint (oil production rate) to the secondary constraint (well bottom hole pressure) as the primary constraint was not satisfied.

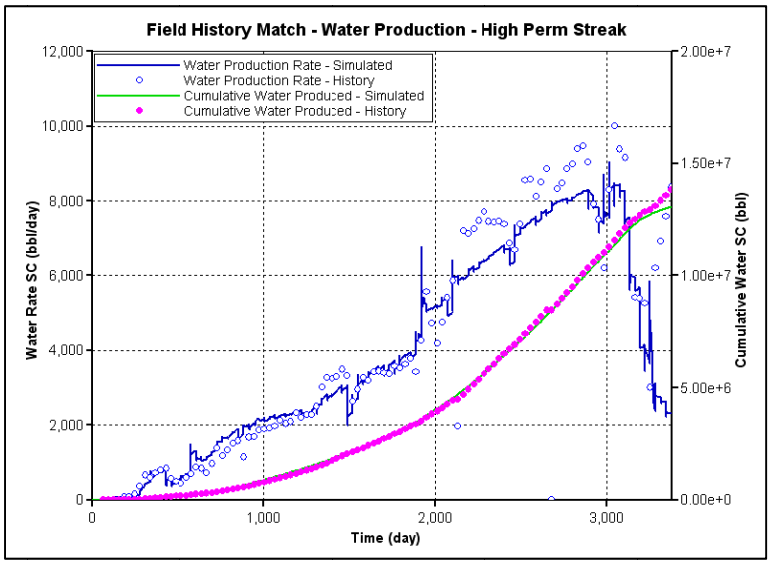

Figure 3.8: Water production history match for reservoir model using 1 Darcy as the permeability of the third layer. History and simulated data do not have a good match after 2000 days due to the simulator switching from primary to secondary constraints.

3.3 Calibrating Breakthrough Time

After the primary depletion period, CO_2 was injected into the reservoir. The CO_2 breakthrough time in producer well, Well #4 was used to calibrate the reservoir model. Actual breakthrough time in the field was approximately one month. During initial runs it took more than one month for breakthrough to occur in the model. Calibration of relative permeability curves was done to bring the simulated breakthrough times closer to one month. Increasing the relative permeability to gas in the presence of liquid (k_{rgl}) was one way to achieve this. But changing this parameter by a large magnitude hinders the relative permeability to oil, and skews the history match. Hence, minor changes to the relative permeability to gas in the presence of water (k_{rgw}) were made to decrease the breakthrough time. APPENDIX B provides the relative permeability plots before history match and after calibration for breakthrough time. Figure 3.9 shows the gas production rate and CO_2 molar production rate for Well #4.

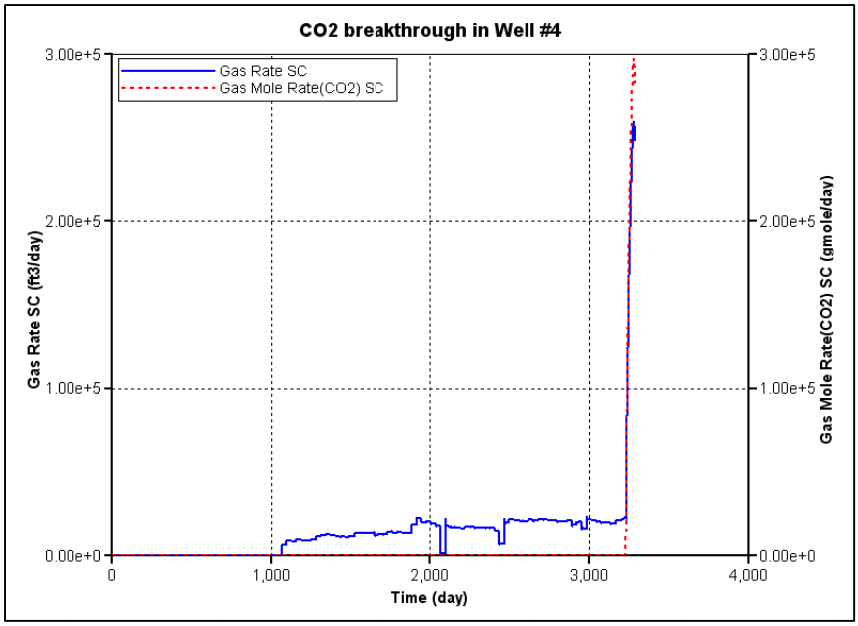

Figure 3.9: CO_2 breakthrough time in producer (Well #4) as observed through gas production rate and CO_2 molar production rate.

4 SWEEP IMPROVEMENT TECHNIQUES

The calibrated reservoir model from the previous chapter was used to investigate techniques which help improve sweep efficiency. This chapter focuses on two such methods; water-alternating-gas (WAG), and profile modification by foam or polymer injection. Firstly, continuous CO_2 injection into the reservoir was simulated. This is the current EOR method employed in the field and was compared with WAG and profile modification.

4.1 Continuous CO_2 Injection

Simulation of continuous injection of CO_2 was used as a base case study for oil recovery from the model. Mitigating methods like WAG and profile modification, which are discussed in the next sections, were compared and studied against the continuous CO_2 injection method.

Continuous CO_2 injection was simulated at an injection rate of 5 MMSCFD, with a constant injection rate as the constraint for the injection well. All five production wells were set to a bottomhole pressure constraint as given in Table 4.1. Since the production rates from Well #3 were higher compared to the other wells, it was given a lower bottomhole pressure constraint. All production wells were set to shut-in when the gas-oil ratio (GOR) reached 50 MCF/STB. The simulations were run for 20 years.

Table 4.1: Production well pressure constraints

Well	BHP Constraint, psia
Well #3	1500
Well #5	2500
Well #4	2500
Well #2	2500
Well #6	2500

Figure 4.1 shows the simulated cumulative oil production from each of the five production wells as well as the cumulative oil production for the field. The plot shows discontinuities in oil production, wherein cumulative field production increases and flattens several times during CO_2 injection. This occurs as a result of the shut-in of production wells due to increased GOR. The sequence in which wells shut-in can be observed from the plot, beginning with Well #3 and ending with the shut-in of Well #6. After Well #3 shuts in, CO_2 moves towards the next nearest producer, Well #4, sweeping oil in between the two wells. Later, Well #4 shuts in due to high GOR enabling CO_2 to move towards Well #3. In this same sequence CO_2 then sweeps the oil between the injector and Well #2, and in the end between the injector and Well #6. Once the GOR of the last producing well, Well #6, goes beyond 50 MCF/STB, the well shuts in and field production stops.

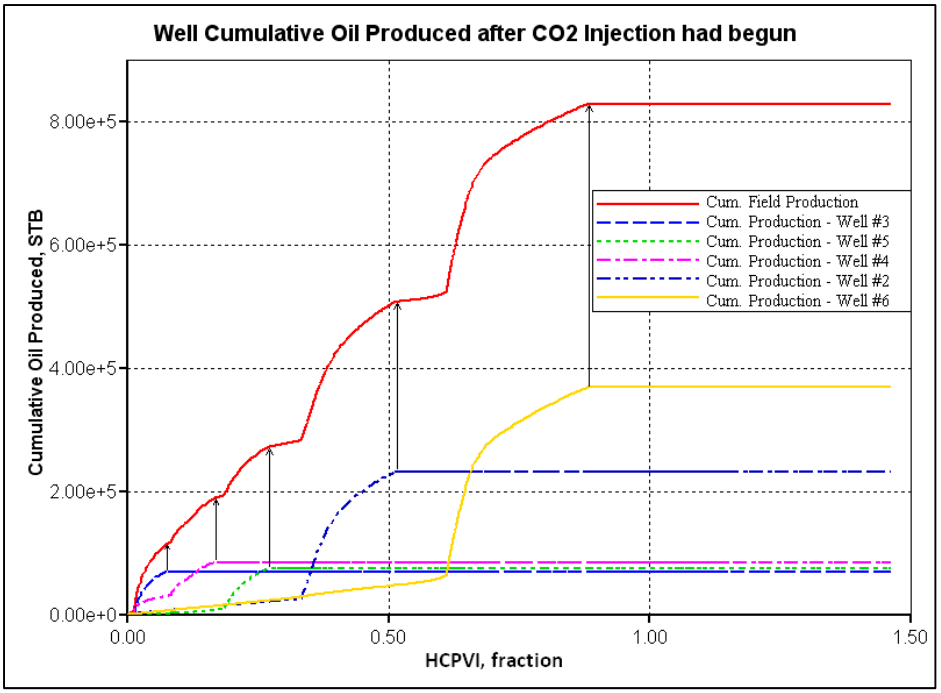

Figure 4.1: Cumulative oil produced from all five producers in the field and overall field cumulative production.

Figure 4.2 shows the variation of global mole fraction of CO_2 in layer 3 with time. Global mole fraction is used as a variable to track the movement of CO_2 in the field. Each map shown in the figure corresponds to the time just before a well shuts in. The third map in the figure (at 4463 days) shows the distribution of CO_2 in layer 3 just before Well #5 has shut-in. After this, CO_2 flows towards the next nearest production well, in this case Well #2, and sweeps the oil which it contacts on the way. This can be seen in the fourth map of the figure (at 5742 days) wherein CO_2 has swept the oil in the region where global mole fraction of CO_2 has increased. Later, Well #2 produces at a high GOR and it shuts in.

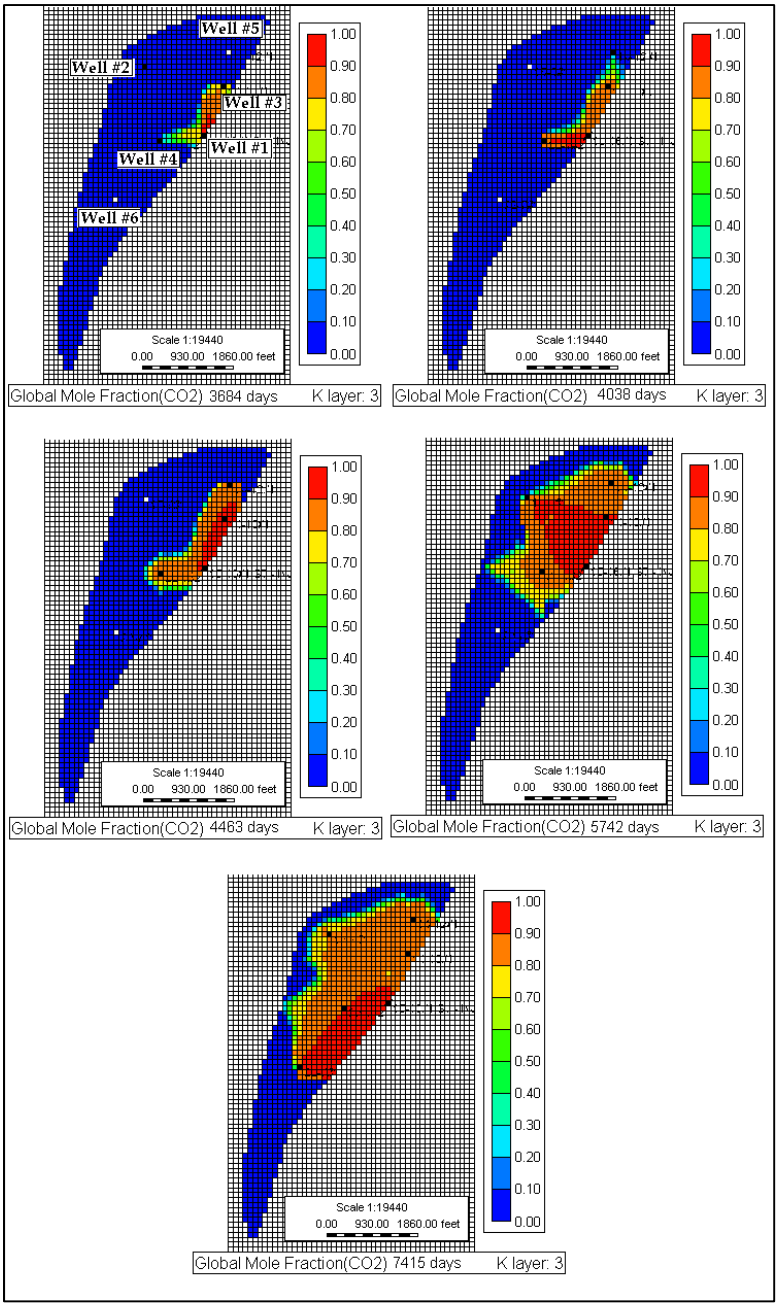

Figure 4.2: Field maps of global composition of CO_2 in layer three of the model. Each maps shows the distribution of CO_2 just before a production well shuts in. Moving from left to right and from top to bottom, each map corresponds to Well #3, Well #4, Well #5, Well #2, and Well #6 respectively.

Now, the CO_2 front moves towards the next low potential region in the field, which is Well #6, sweeping oil in its path. Map 5 in the figure (at 7415 days) shows the region contacted by CO_2 while flowing towards Well #6.

Ideally, in a homogenous reservoir, a standard pattern flood such as an inverted 5-spot pattern would be utilized. In such a pattern all four production wells will start and stop oil production at approximately the same time. This is due to the similar distances between the injector and producers. However, in this field, wells are not in any regular pattern, which resulted in different production wells breaking through and shutting in at different times.

4.1.1 Oil Recovery

Continuous injection of CO_2 recovers an incremental 7 percent of the OOIP. This recovery is lower than the recovery obtained from other CO_2 flooded fields (EOR Field Case Histories, 1987). However, a closer examination reveals that heterogeneity plays a major role in recovering lower quantities of oil. Table 4.2 provides layer-by-layer oil recovery values from the 5 layers defined in the reservoir model.

Table 4.2: Layer wise oil recoveries after CO_2 flood

	Primary Recovery, % OOIP	CO_2 Flood Incremental Recovery, % OOIP	Overall Recovery, % OOIP
Layer 1	3.6	0.7	4.3
Layer 2	6	14.3	18.6
Layer 3	21.9	26.8	48.7
Layer 4	27.9	-1.3	26.6
Layer 5	31.7	-1.1	30.6

Stripping of lighter fractions of oil is observed as one of the mechanisms of recovery. These observations are similar to the ones described by Spivak and Chima (1984) and seen in the slimtube simulations in Chapter 2. Figure 4.3 shows a plot of gas mole fraction of C_1 in two grid blocks [24, 22, 3] and [27, 28, 3], where the first grid block is farther from the injection well than the second grid block. It shows a sudden increase in the mole fraction of C_1 in the gas phase in both the grid blocks which confirms the stripping of lighter components out of the oil phase, and these stripped components form a bank at the leading edge of the front.

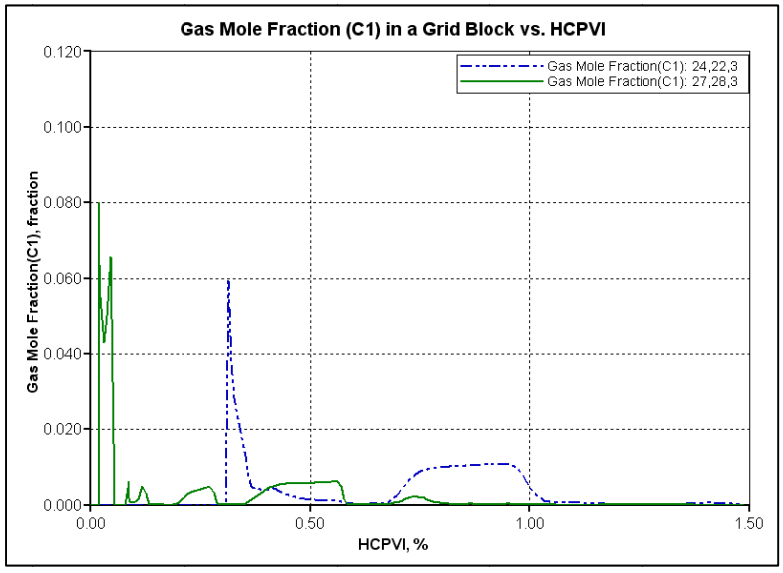

Figure 4.3: Variation of gas mole fraction of C_1 component in two grid blocks shows stripping of lighter fractions.

Oil production in continuous CO_2 injection occurs primarily due to CO_2 contacting oil in layer 3. It was also observed that almost the entire amount of gas injected goes into layer 3 (Figure 4.4). This is obviously due to the presence of extremely high permeability in layer 3.

Figure 4.5 shows the oil recovery from perforations for each of the 5 layers. Oil recovery from perforations is defined as the ratio of cumulative oil production from the perforations in a layer to the original volume of oil in the layer at time 0 (Computer Modeling Group, 2011). This figure shows that most of the oil was produced from layer 3, and a very small quantity was produced from the remaining layers. This is possible only if oil migrates into layer 3 from the other 4 layers. Oil migration between the layers is difficult to track. Figure 4.6 shows the oil recovery from each layer using the actual definition of oil recovery. This definition is the ratio of cumulative oil removed from a layer (produced or migrated) to the original volume of oil in a layer at time 0. Figure 4.6 shows that at the time of field shut-in, layers 1, 4, and 5 have approximately the same amount of oil remaining as they had before the beginning of the CO_2 flood. In contrast, oil has been removed from layer 3 and 4. Hence, from Figure 4.5, Figure 4.6, and layer recovery values from Table 4.2 we can conclude that oil migrates from layer 3 to layer 4. Moreover, the negative recovery values for layer 4 and layer 5 was believed to be a result of migration of low viscosity oil from layer 3 due to gravity.

4.1.2 Reservoir Extent Contacted by CO_2

Contact of reservoir rock by CO_2 is an indicator of the extent of sweep, both vertical and areal, achieved by the CO_2 injection process. Global mole fraction of CO_2 was used to study the 3D maps of the model to locate the areas in the reservoir contacted or blocked from contact by CO_2.

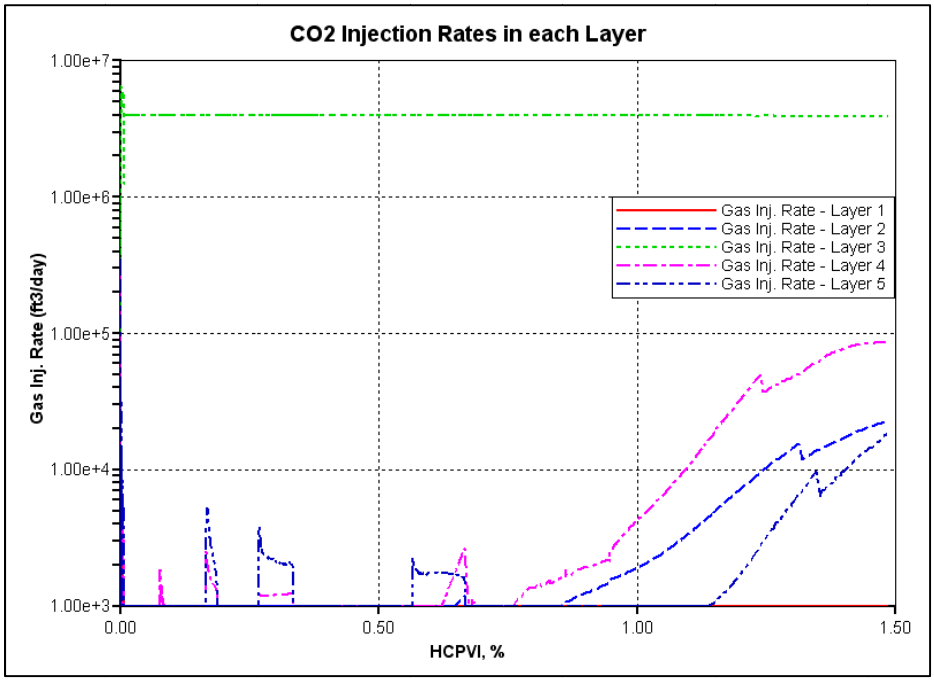

Figure 4.4: CO_2 Injection Rates in each layer for continuous gas injection

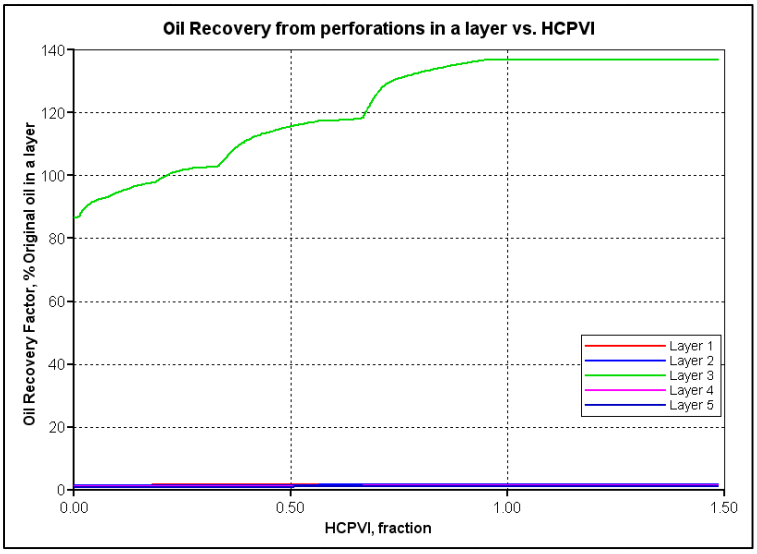

Figure 4.5: Oil recovery factors based on the oil produced form each layer, and is expressed as the ratio of oil produced from the well perforations in a layer and the original amount of oil in a layer at time = 0. Layer 3 has a very high recovery (>120%). Hence, oil from other layers must move into layer 3.

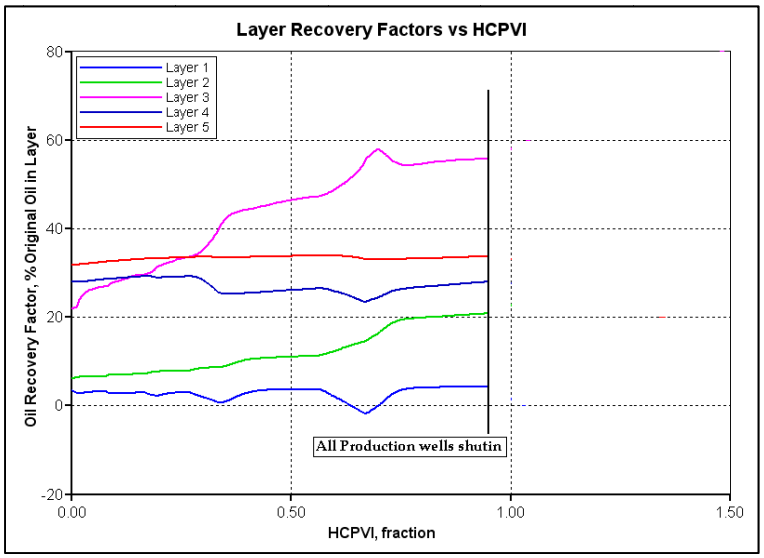

Figure 4.6: Oil recovery factors for each layer expressed as the ratio of oil removed (produced or migrated) from a layer and the original amount of oil in a layer at time 0. Layer 3 has a very high recovery (>55%), implying very less remaining oil saturation in layer 3. Layer 1, 4 and 5's recovery is approximately the same as what it was before CO_2 injection, implying that oil has moved into this layer.

Figure 4.7 shows the global mole fraction of CO_2 in all 5 layers in the model at the end of CO_2 flooding. Due to the very high fraction of CO_2 injected into layer 3, CO_2 sweeps oil primarily out of layer 3. However, the discrepancy in incremental oil recoveries from layers 2 and 4 can be explained by the effect of gravity. It was observed through oil saturation maps that CO_2 migrated from layer 3 to layer 2. This can be explained as a gravity effect. Also, CO_2 decreases the viscosity of oil it comes into contact with. Figure 4.8 shows the viscosity of oil contacted by CO_2 in layers 2 and 4, where viscosity decreases to less than 10 cp. This decrease in viscosity could also be one of the reasons for migration of oil between layers.

Migration of CO_2 between layers was not observed as long as the CO_2 front remains in layer 3. CO_2 does not migrate into different layers until production wells are shut in, due to high GOR. Once a well is shuts in, CO_2 flows vertically from layer 3 to layer 2 and layer 4. This is also the duration when the CO_2 front moves towards the next production well in layer 3. Figure 4.9 and Figure 4.10 show a schematic of CO_2 migration into other layers. Figure 4.9 shows the CO_2 front when it has reached the closest production well. Once the production well GOR increases to 50 MCF/STB, the well shuts in, and the CO_2 front moves towards the next production well. During the time when the CO_2 front moves, CO_2 migration into layer 2 and 4 was observed, and as soon as the CO_2 front hits the next production well, CO_2 migration into other layers ceases (Figure 4.10).

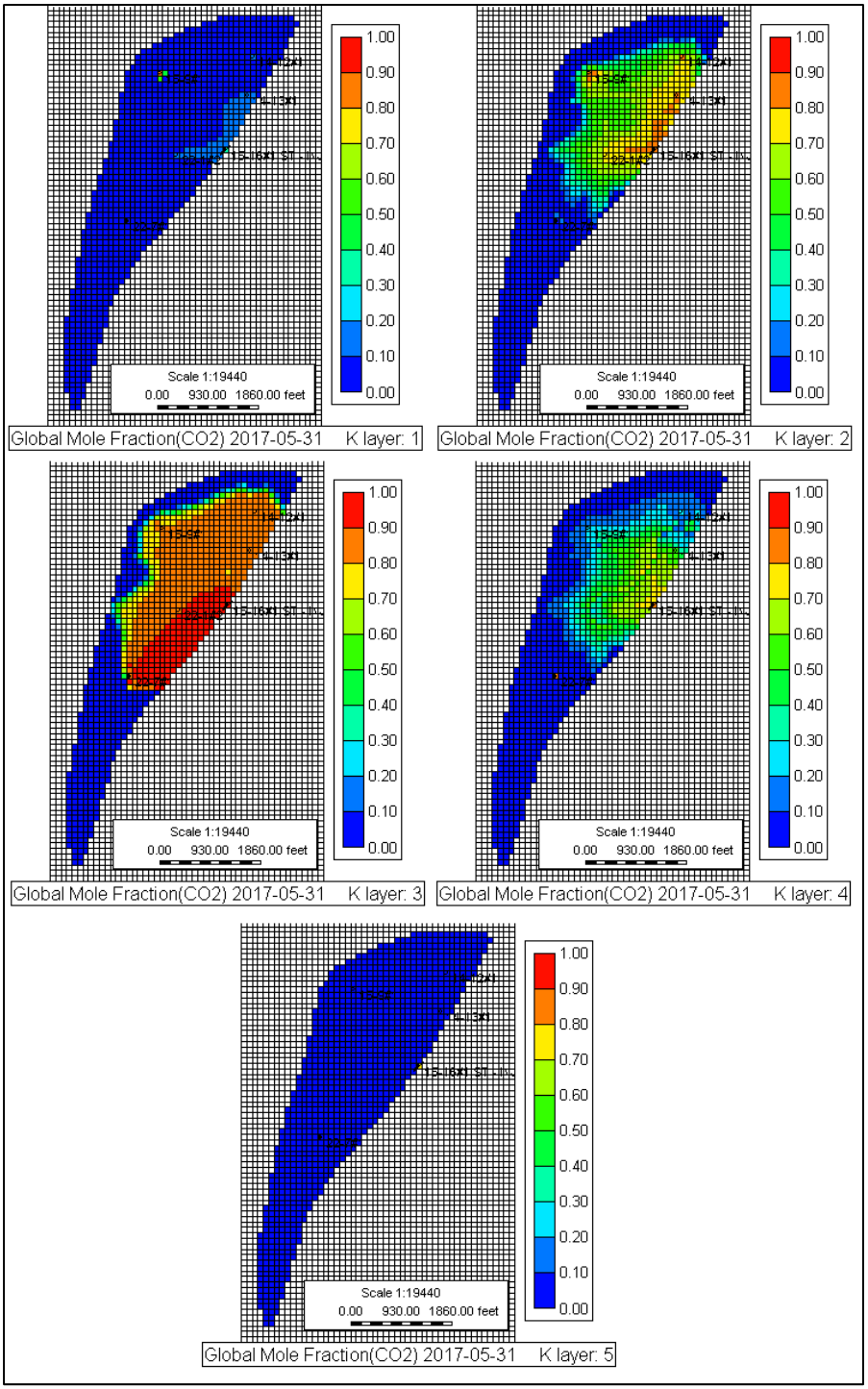

Figure 4.7: Global mole fractions of CO_2 in all 5 layers of the model after CO_2 flooding had been stopped.

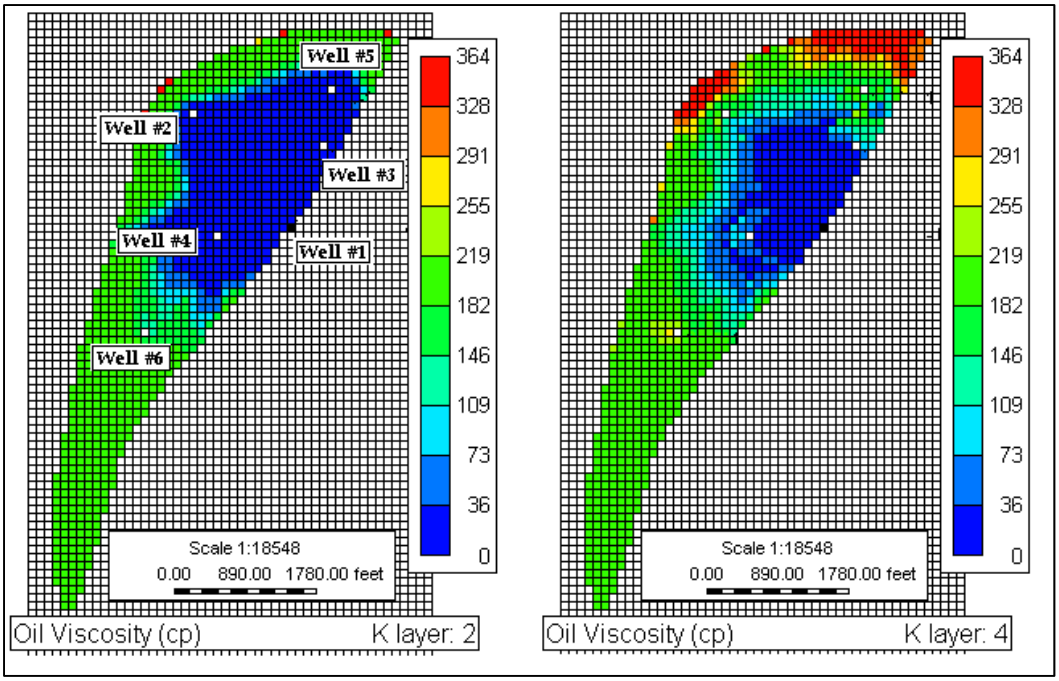

Figure 4.8: Oil viscosity of CO_2 contacted oil in layers 2 and 4. This substantial decrease in oil viscosity is may be one of the reasons of oil migration between layers.

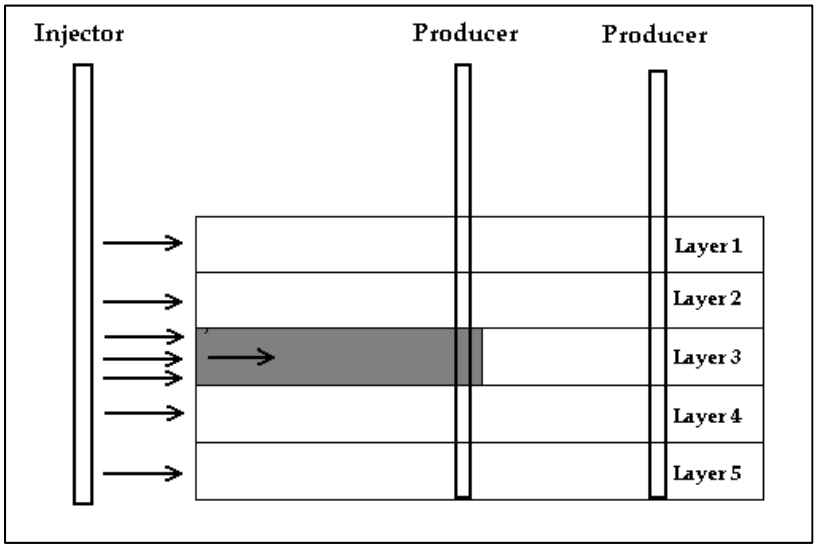

Figure 4.9: Schematic diagram of CO_2 front movement in layer 3. Producer well nearest to the injector well shuts in after the GOR reaches 50 MCF and CO_2 front moves towards the next producer well.

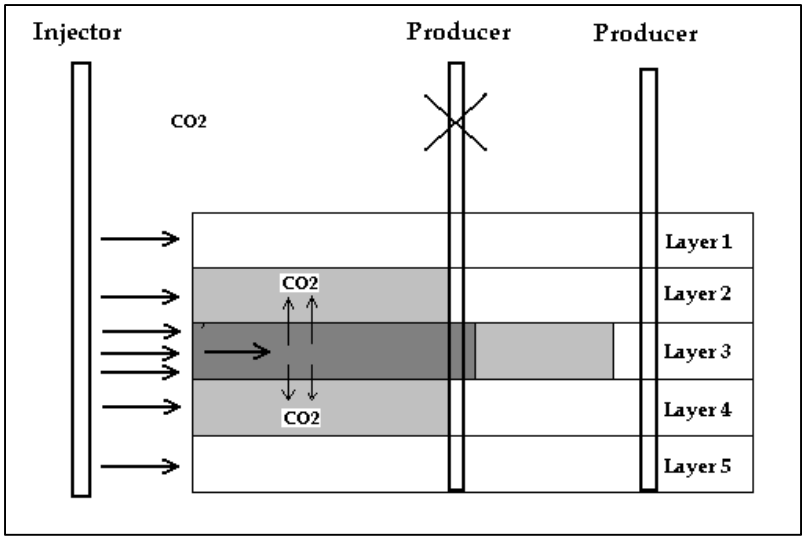

Figure 4.10: Schematic diagram of CO_2 movement in layer 3 and migration from layer 3 to layer 2 and 4. Once the nearest producer well shuts in, CO_2 front moves to the next producer well, and CO_2 also migrates into other layers.

4.2 Water-Alternating-Gas (WAG)

WAG processes employed in the field have often shown better recoveries compared to the continuous gas injection process. Improved mobility control and lower carbon dioxide requirements make WAG methods promising for heavy oil reservoirs (Dyer and Ali, 1989; Mangalsingh and Jagai, 1996). Heterogeneity (stratification and anisotropy) has been documented as a major factor affecting WAG performance (Surguchev, et al., 1992). Apart from heterogeneity, wettability and fluid properties also affect the results of a WAG process.

The WAG ratio is the ratio of volume of water injected to the volume of gas injected at reservoir conditions (Green and Willhite, 1998). Rojas and Farouq Ali (1986) and Mangalsingh and Jagai (1996) reported a WAG ratio of 1:4 to be the most optimal of the

several WAG ratios which they had conducted experiments on. These experiments were conducted using heavy oils with oil gravity ranging from 14° API to 29° API.

For the work presented here simulation runs for several WAG ratios were conducted on the reservoir model. Two different sets of WAG ratios were evaluated, one in which the CO_2 slug size was greater than the water slug size (WAG ratios of 1:1 to 1:5), and the other in which the water slug size was greater than the CO_2 slug size (WAG ratios of 2:1 and 3:1). In these simulations a WAG ratio of 1:1 represents injecting water for a month at a constant rate (2500 bbl/day) and then injecting CO_2 at a similar reservoir rate (5 MMSCFD) for a month, which equates to an approximate slug size of 0.85% HCPV.

4.2.1 Oil Recovery

In each of these simulations, WAG injection began at the same time as CO_2 injection began in the field. Production well constraints were the same as were used for the continuous gas injection.

Table 4.3 provides a brief description of the different methods tested in these simulations. Figure 4.11 shows the cumulative oil produced for hydrocarbon pore volumes injected. The non-uniform and unsmooth nature of the recovery curves is due to the varying distances between the injector well, and the producer wells. As the oil bank reaches a producer a corresponding steep increase in the recovery is observed, and over a period of time, the recovery curve gradually flattens. These observations are similar to what was described in the previous section on continuous CO_2 injection.

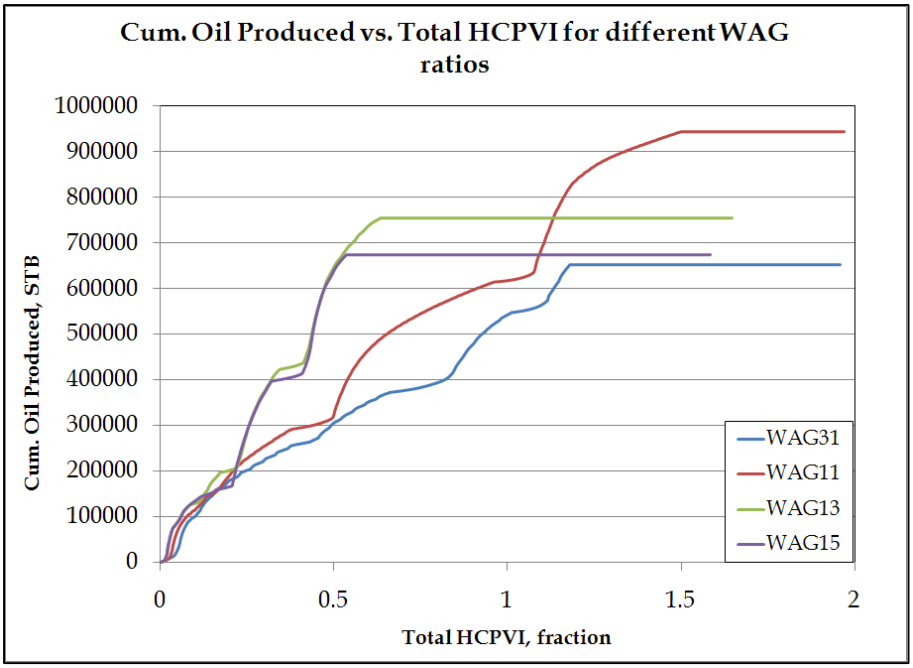

Figure 4.11: Cumulative oil produced for different WAG ratios. WAG ratio of 1:1 was found to give the highest recovery.

It can be noticed from Figure 4.11 that a WAG ratio 1:1 results in highest recovery. The mechanism of oil recovery by WAG was difficult to understand using the reservoir model. Hence, core flood simulations were conducted to determine the recovery mechanisms.

4.2.1.1 Mechanism of Oil Recovery

In order to understand the recovery mechanisms using WAG, core flood simulations were conducted. A 1-D simulation model similar to the slim tube simulation model discussed previously was used. All simulations were conducted at 3500 psi. The injector was set a constant rate constraint of 0.0001 bbl/day. This rate constraint was set at bottomhole

conditions during gas slug injection, and during water injection the same injection rate constraint was set at surface conditions. The producer well was set to a bottom hole pressure constraint of 3500 psi. A slug size of 1% HCPV was injected in each cycle.

Table 4.3: Description of different WAG simulation runs

Simulation run	Remarks	Cutoff GOR (MCF/STB)	CO_2 Inj. Rate, MMSCFD	Water Inj. Rate, bbl/day	Incremental Recovery (% OOIP)
WAG 3:1	3 months water and 1 month CO_2 cycles	50	5	2500	7.4
WAG 1:1	1 month water and 1 month CO_2 cycles	50	5	2500	10.8
WAG 1:3	1 month water and 3 months CO_2 cycles	50	5	2500	8.6
WAG 1:5	1 month water and 5 months CO_2 cycles	50	5	2500	7.6

During core flood simulations it was observed that CO_2 decreases the viscosity of oil and later water acts as a displacing fluid and pushes oil towards the producer. Figure 4.12 shows the oil viscosity, water saturation, and gas mole fraction of the C_1 component in a grid block. This grid block is approximately 10.7 ft from the injection end of the core flood simulation. The increase in mole fraction of C_1 shows the stripping of lighter fractions in the oil by CO_2. This along with CO_2 dissolving in oil decreases the viscosity of oil from 178 cp to

approximately 10 cp. Water which follows the slug of CO_2 displaces the oil towards the producer. This was also observed in experimental studies on heavy oil by Zhang et al. (2006).

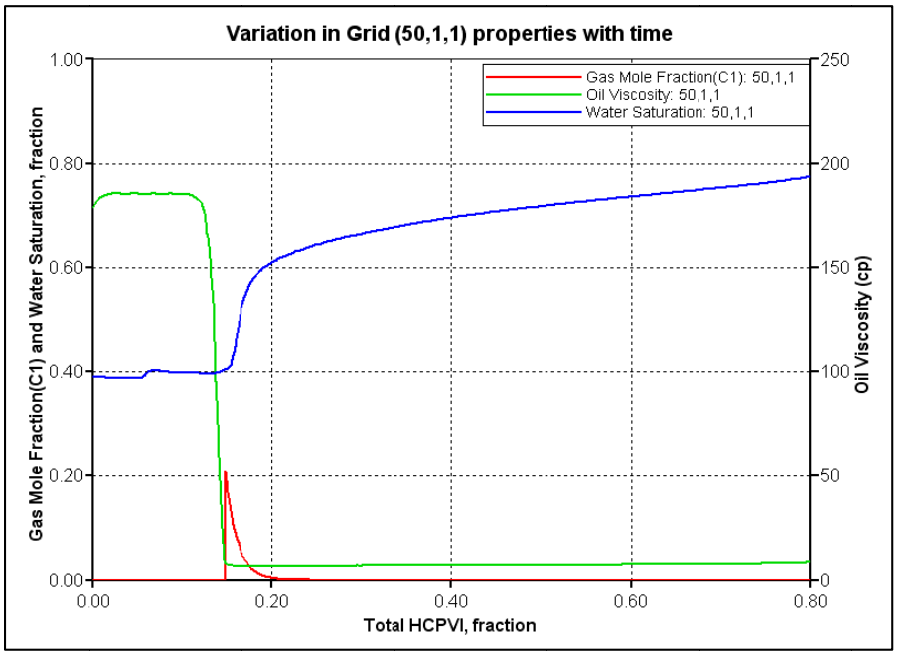

Figure 4.12: Variation of oil viscosity, water saturation, and mole fraction of C_1 in gas in grid block 50,1,1. The plots shown in this figure are for a WAG ratio of 1:1.

Similar plots (Figure 4.13) for a grid cell near the producer well with grid block address 250,1,1 shows an increased mole fraction of C_1 in the gas phase. This shows that as CO_2 contacts more oil, it strips more lighter fractions.

Since this is a WAG process, the saturation of water in a grid block was expected to increase and decrease according to the slug of fluid being injected. But this response was not observed in either of the figures (Figure 4.12 and Figure 4.13). Due to the very small injection

rates, it is believed that injected CO_2 dissolves in the water phase and hence does not form a CO_2 bank. As a result, continuously increasing water saturation is observed behind the flood front. However, simulation of a WAG ratio of 1:5 showed the intermittent increase and decrease of water saturation behind the flood front due to the larger slug size of CO_2 used.

Table 4.4 shows the oil recoveries after injecting 1.2 HCPV for three WAG ratios which were tested during core flood simulations. It can be noticed that WAG ratios greater than 1 resulted in better recoveries compared to simulations where the WAG ratio was less than 1; however the highest recovery was obtained for a WAG ratio of 1:1. The same trend was observed during WAG simulation runs using the full field reservoir model. This is different from field studies of WAG in light oil reservoirs. WAG ratio of 1:2 (EOR Field Case Histories, 1987; Senocak, 2008; Li, et al., 2003) is often reported to yield the highest oil recovery.

Table 4.4: Oil recovery for different WAG methods during core flood simulations

Method	Recovery after 1.2 HCPVI, % OOIP
WAG 3:1	76
WAG 1:1	82
WAG 1:3	70
WAG 1:5	65

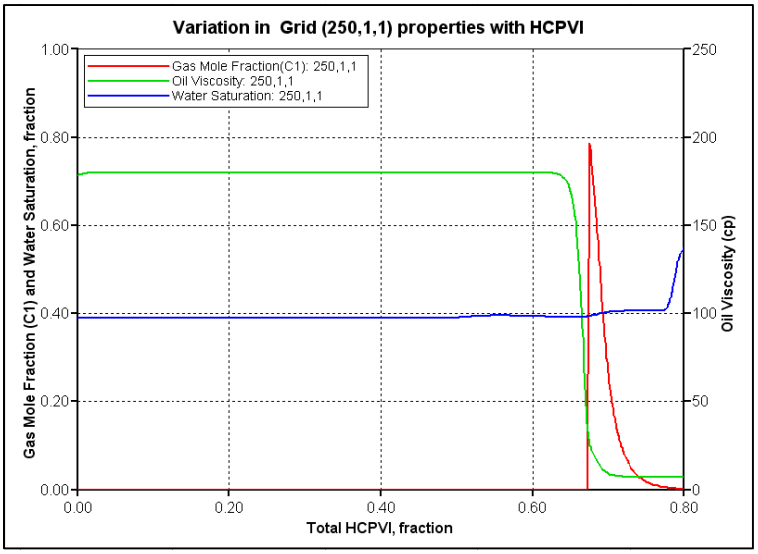

Figure 4.13: Variation of oil viscosity, water saturation, and mole fraction of C_1 in gas in grid block 250,1,1. The plots shown in this figure are for a WAG ratio of 1:1.

4.3 Profile Modification

Profile modification is achieved by using different types of 'blocking agents' which are injected into a targeted layer. These blocking agents could be foam, gels or polymers.

The effect of foam on the permeability of a porous media to gas has been studied by several researchers and was also tested in field cases (Bernard and Holm, 1964; Holm and Garrison, 1988). Injection of foam causes a significant reduction of the relative permeability to gas, and this reduction is dependent on parameters like foam quality and texture, temperature, and time (Llave, et al., 1990; Di Julio and Emanuel, 1989). Three sets of experiments conducted by Llave, et al. (1990) have shown that the final relative permeability to gas with foam at residual water saturation was 10.2%, 2.5%, and 2.8% of the relative

permeability value of gas with brine. This decreased relative permeability to gas was utilized as a blocking agent in layer 3 of the reservoir model and decreased the relative injection and/or flow of CO_2 into this layer.

4.3.1 Exporting and Validating the Fluid Model to CMG-STARS®

STARS® is CMG's advanced processes reservoir simulator which includes options to simulate processes which GEM® does not. For the purposes of this work these processes included chemical flooding and foam injection (Computer Modeling Group Ltd., 2009). In STARS®, fluid component interactions are characterized by equilibrium coefficients between components or k-values. The existing fluid model was converted into a STARS® compatible model using WINPROP® to generate k-values between pseudo-components.

Since the fluid model was changed, there was a need to test the k-value fluid model for its consistency with some of the existing data. The slimtube simulation data was used to test this. Slimtube simulation runs using the k-value fluid model at 7000 psia indicated that recoveries did not exceed 50%, whereas simulation recovery at the same pressure using the Peng-Robinson model was 91%. However, it was observed that the mole fraction of heavier pseudo-components (C_6-C_{12}, C_{13}-C_{35}, C_{36}^+) remaining at the end of simulation was very high (51%, 47%, 46% respectively). Hence, k-values were manually changed for these three pseudo-components and slimtube simulations were re-run. After a set of 30 trials in which k-values for these three pseudo-components were changed between factors of 10^{-4} and 10^6, the highest recovery obtained was 66%. After consultation with support personnel at CMG, this

issue was not resolved conclusively. Hence, a different method needed to be developed to simulate injection of a blocking agent in the reservoir.

4.3.2 Method to Replicate Foam in CMG-GEM®

Due to the problem in replicating the results of slimtube simulation using the k-value fluid model, a work-around method to model the properties of a blocking agent in GEM® was opted for. This method consisted of defining a different rock type (Rock Type 2) near the injection well (Well #1) in layer 3 of the reservoir model, and using a different set of relative permeability tables which are indicative of the relative permeabilities in the regions where the blocking agent is active.

Three different relative permeabilities for Rock Type 2 were considered and these relative permeability values were assumed to remain constant throughout the life of the CO_2 flood which followed the placement of the "blocking agent". In foam flooding field projects, relative permeabilities vary with time and are dependent on foam quality, temperature and many other parameters. Very often the relative permeability data is hard to measure experimentally, hence production data is analyzed and history matched to generate suitable relative permeability data.

Several simulation test cases were run to simulate "foam injection" in the model. Two different gas relative permeabilities, 1%, and 3% of gas relative permeability in brine, were used to generate two sets of relative permeability tables. Areal coverage of the zone injected with blocking agent was varied to replicate three different radii of foam penetration, and

tested for the sensitivity of the injection distance to incremental oil recovery. Also, three different CO_2 injection rates; 4, 5, and 6 MMSCFD, were used to study sensitivity on injection rate. Figure 4.14 shows one such case where the distance of blocking agent penetration in layer 3 is approximately 600 ft from the injection well, and Figure 4.15 shows the gas-liquid relative permeability curve in which the relative permeability of gas in the presence of the blocking agent, k_{rg}, is 5% of the relative permeability of gas in the presence of brine.

4.3.3 Oil Recovery

The presence of blocking agent in layer 3 hinders the flow of CO_2. As a result, CO_2 contacts the reservoir rock in layers 1, 2, 4 and 5 more so than in the continuous injection and WAG cases. All the plots discussed here are for the case which has a gas relative permeability in 'Rock Type 2' which is 3% of the gas relative permeability with brine, and the areal extent of the blocked region is as shown in Figure 4.14.

Injecting blocking agent into layer 3 achieved success and this was due to the properties of a profile modifying agent. Blocking agent restricts gas injection into layer 3 and directs gas to flow into the other 4 layers. Figure 4.16 shows the layer-wise injection rates. Injection rates in each layer are distributed approximately according to the gas permeability in each layer.

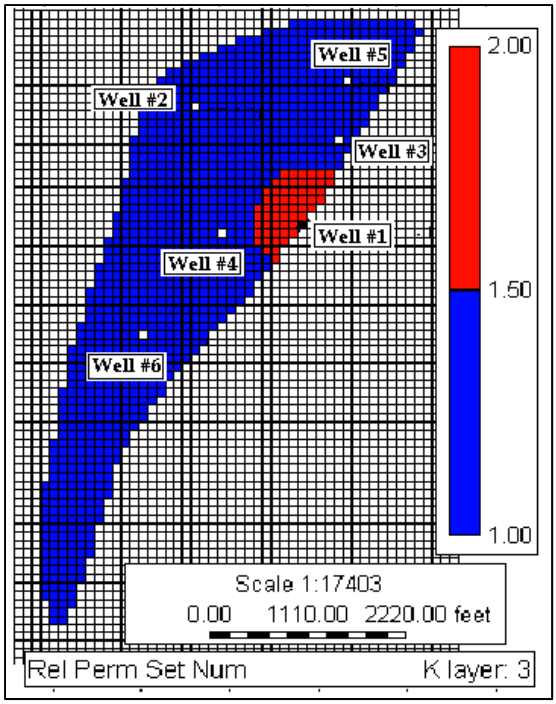

Figure 4.14: Reservoir map showing two different rock types. 'Rock Type 2' (shown in red) is used to replicate the zone injected by blocking agent.

CO_2 injected into layer 4 initially flows in that layer. As shown in Figure 4.17 after injecting for a few years, and once the CO_2 in layer 4 has surpassed the areal extent of the blocked region, CO_2 migrates into layer 3. Beyond the blocked region, layer 3 has an increased effective gas permeability which makes it easier for CO_2 to flow in layer 3. This enables the CO_2 to cross into layer 3 and migrate to the producer.

Once CO_2 has entered layer 3, it acts like a regular CO_2 flooding process, and shows the same behavior as was observed in continuous gas injection. Hence, the effect of the blocking agent is no longer felt beyond the blocked region, and the farther the blocking agent is placed in layer 3 the better the sweep in layers 2 and 4.

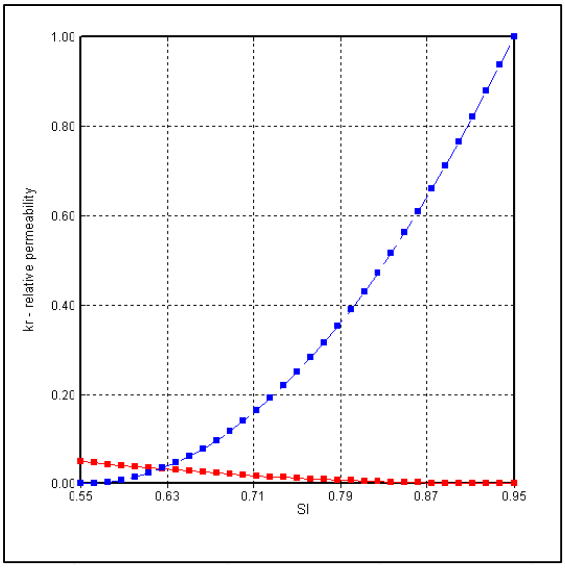

Figure 4.15: Gas-liquid relative permeability curve used for 'Rock Type 2' shown in Figure 4.14

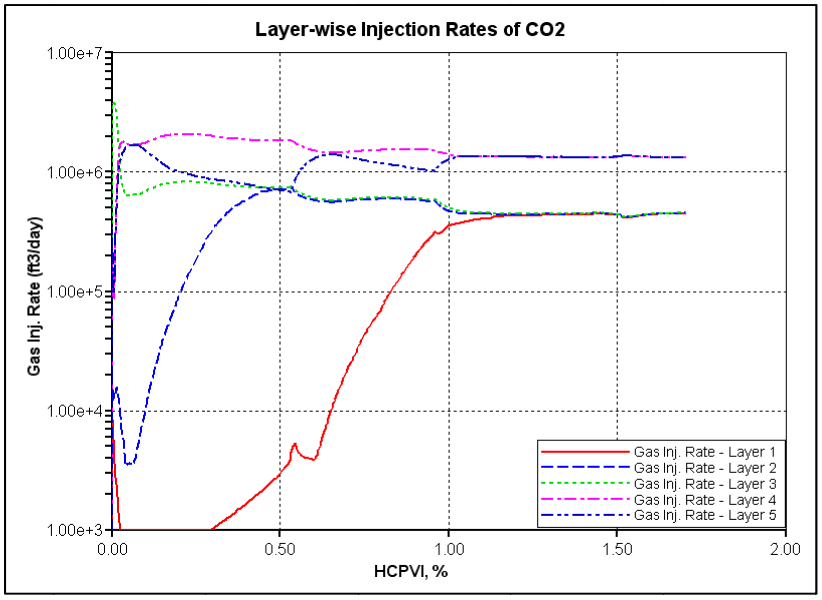

Figure 4.16: CO_2 injection rates into each of the 5 layers in the reservoir.

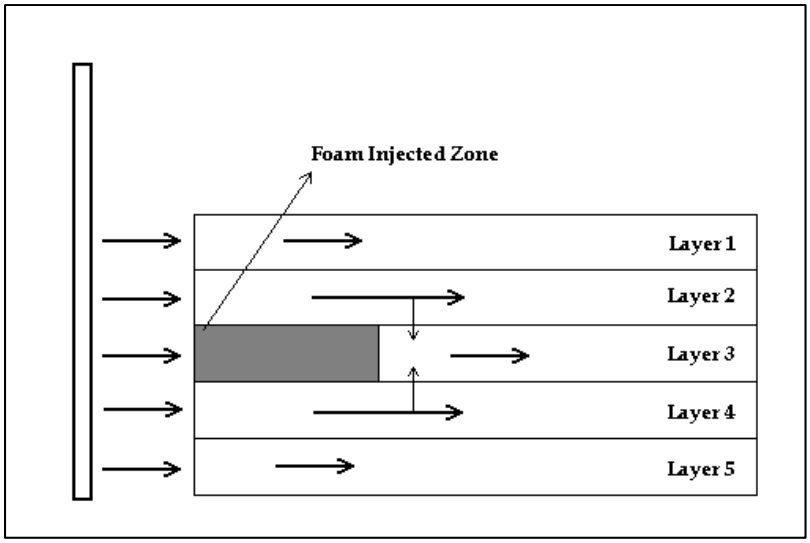

Figure 4.17: Schematic diagram of flow of CO_2. After surpassing the zone injected by blocking agent, CO_2 in layer 2 and 4 flows into layer 3. Figure not to scale.

The volume of rock contacted by CO_2, which is represented using the global mole fraction of CO_2 in a grid block, is greater in the case of profile modification when compared with CGI and WAG. Figure 4.18 shows the layer maps of grids contacted by injected CO_2 for all the 5 layers. It was observed that CO_2 has swept a portion of rock in both layer 1 and 5 which was not contacted by CO_2 in the previous cases.

4.3.4 Radius of Injection of the Blocking Agent

As noted above, the larger the areal extent of layer 3 blocked, the better the sweep efficiencies achieved by injected CO_2. Blocking agent was placed at three different radii from

the injection well and CO_2 flooding was carried out to study the sweep of oil and the eventual recoveries.

Figure 4.19 shows very high incremental recoveries if the blocking agent is placed for a larger areal extent. The greater recovery can be explained by the schematic shown in Figure 4.17 where, as the areal extent increases, CO_2 pushes the oil in the top and bottom layers resulting in better sweep efficiency in these layers. The gas relative permeability in the region blocked is 1% of the gas relative permeability in the unblocked region. The data points referring to zero radius of placement of blocking agent corresponds to continuous CO_2 injection. Figure 4.20 shows a plot similar to the one in Figure 4.19, but with the gas relative permeability in the region blocked at 3% of the gas relative permeability in the unblocked region.

It must be noted that increasing the areal extent of the blocking agent is a difficult process. As will be shown, pressure drop between the wells increases in the simulations. If the chemicals used in the blocked region cannot stand these higher pressures, the stability of the blocked region will be compromised. If the blocking agent can withstand these pressures, it is unlikely that placement deep into the reservoir will be possible as the near well pressures would grow to unreasonably high values.

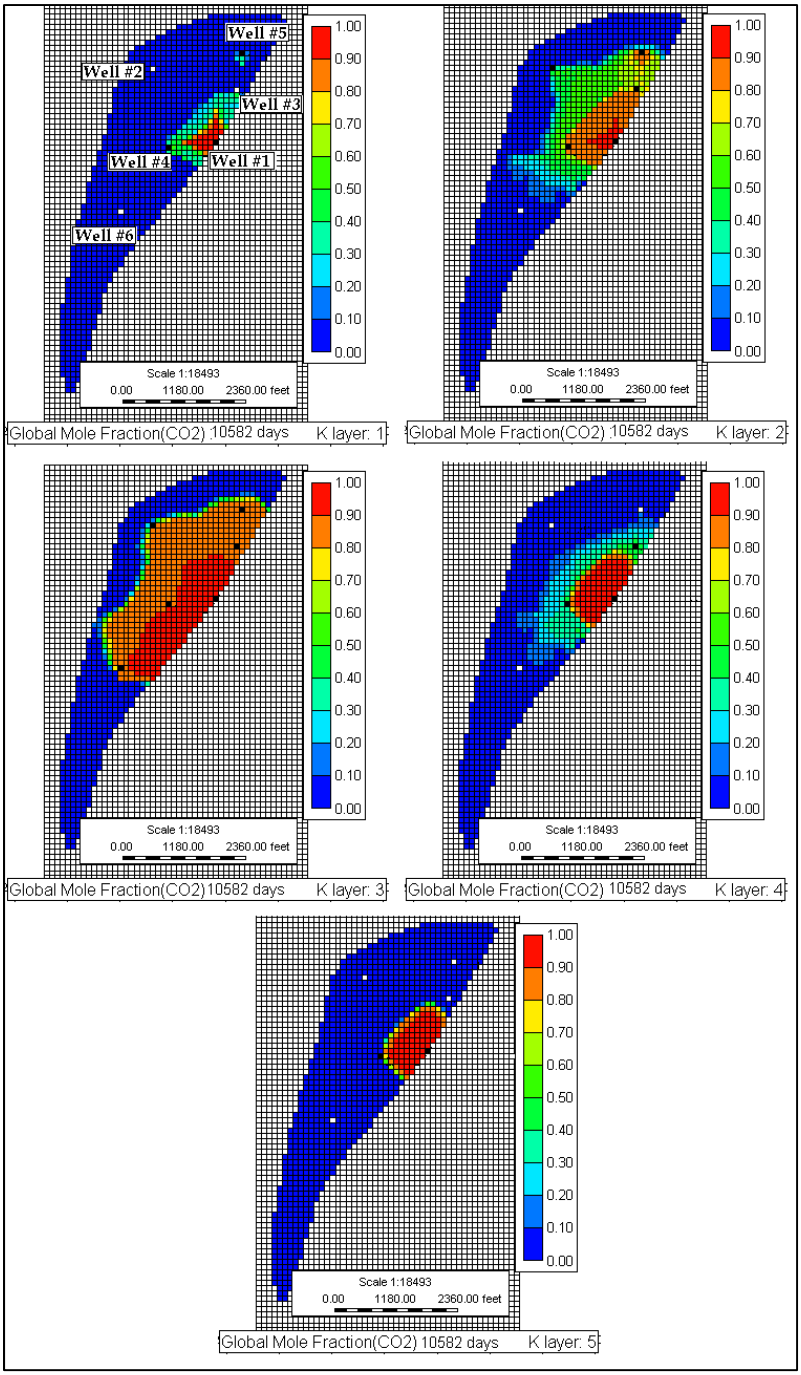

Figure 4.18: Global mole fractions of CO_2 in each layer at the end of oil production in profile modification method. Global mole fraction of CO_2 is used to represent the rock volume contacted by CO_2.

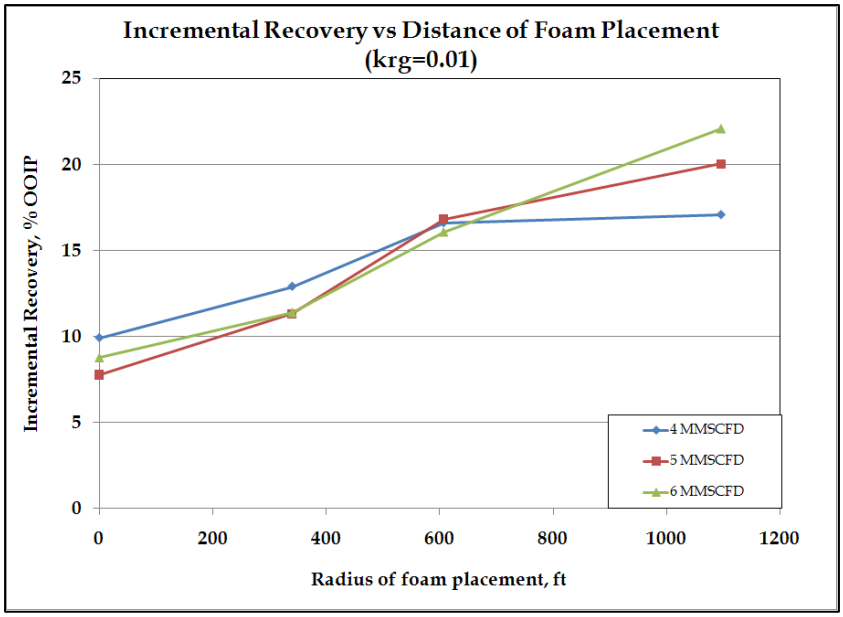

Figure 4.19: Incremental Oil recovery for different distances of placement of the blocking agent. k_{rg}=0.01

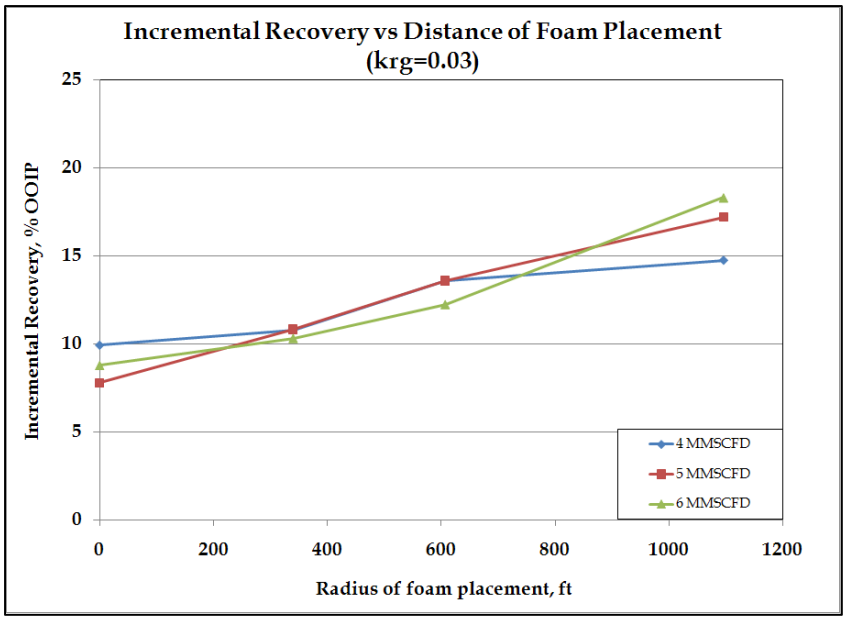

Figure 4.20: Incremental Oil recovery for different distances of placement of the blocking agent. k_{rg}=0.03

4.4 Comparison of Methods

This section of the chapter compares and contrasts the three methods studied above on several parameters. Some of the parameters which were considered were, oil recoveries, pressure differences between grid blocks, gas breakthrough times, and improvement in layer injection rates. These parameters are studied to understand the effect each of the above described methods have on their suitability in field applications for recovering heavy oil.

4.4.1 Oil Recovery

Oil recoveries were found to increase between CGI and WAG, and between WAG and profile modification. Recovery was the highest for profile modification and was found to increase as the radius of placement of the blocked area increases. Table 4.5 summarizes the oil recoveries for each of the three methods tested during this work.

As discussed in the previous section, oil recovery by WAG increases due to the two step process, firstly, the effect of stripping of lighter oil components, viscosity reduction and swelling caused when CO_2 comes into contact with oil, and secondly, the displacement of low viscosity oil by water. This was also observed in core flood experiments of CO_2 floods and WAG. Oil recovery after injecting 1.2 pore volumes of CO_2 was 63%, whereas the same for WAG with a 1:1 ratio was 83%. Also, the areal extent of rock volume contacted by the injected fluid (CO_2 and water) was approximately the same for both CGI and WAG. The rock volume contacted was estimated by visual inspection.

Table 4.5: Summary of oil recoveries from the methods tested in this work. Blocking Agent 1, 2 and 3 correspond to increasing areas of blocking agent injected into layer 3.

Method	Total Recovery, % OOIP	Incremental Recovery over Primary Depletion, % OOIP	Incremental Recovery over CGI, % OOIP
Primary Depletion	18.5	N/A	N/A
CGI	25.5	7	N/A
WAG 3:1	25.9	7.4	0.4
WAG 1:1	29.4	10.9	3.9
WAG 1:3	27.2	8.7	1.7
WAG 1:5	26.2	7.7	0.7
Blocking Agent 1	29.4	10.9	3.9
Blocking Agent 2	32.1	13.6	6.6
Blocking Agent 3	35.7	17.2	10.2

Profile modification showed a substantial improvement in oil recovery mainly due to the diversion of injected gas into layers 1, 2, 4 and 5. This allowed improved sweep in these layers which were otherwise unswept in CGI and WAG. Moreover, as shown in Figure 4.19 and Figure 4.20, recovery increases as the area of the blocked zone in layer 3 increases, and also as a better blocking agent is placed which decreases the gas relative permeability.

4.4.2 Pressure Difference

Pressure drop values between the bottom hole pressure of the injector and an adjacent grid block were plotted to see how they vary. This grid block (33,25,3) was 200 ft away from the injector well (33,27,3) in layer 3. Figure 4.21 shows the pressure difference between these

two grid blocks. The WAG method shows a periodic increase in pressure drop, which occurs when a slug of water is injected. On an average the pressure drop gradually increases as we move from CGI to WAG and then to profile modification, which means that the effective mobility of the injected fluid (k/μ) decreases as we move from CGI to WAG to profile modification. For each of the cases discussed here, the rate of injection, area of flow, and the distance between the two pressure readings are the same, hence from Darcy's Law, pressure difference and mobility are inversely proportional. Therefore, as the pressure difference increases the effective mobility ratio decreases making it easier to displace the oil.

4.4.3 Gas Breakthrough Time

An early breakthrough of injected CO_2 is not desirable in any CO_2 EOR project. The current reservoir model has a relatively early gas breakthrough time due to the presence of the high flow capacity region (layer 3), and that the distance between the injector and the nearest producer is fairly small.

Each of the EOR methods discussed above was found to delay the gas breakthrough time when compared to that found in the continuous CO_2 injection case. Table 4.6 gives the hydrocarbon pore volumes injected in each case before gas breakthrough was observed. The WAG method with a WAG ratio greater than 1 was found to have the largest time to breakthrough. This is due to the low amount of CO_2 injected into the reservoir compared to the total amount of pore volumes injected.

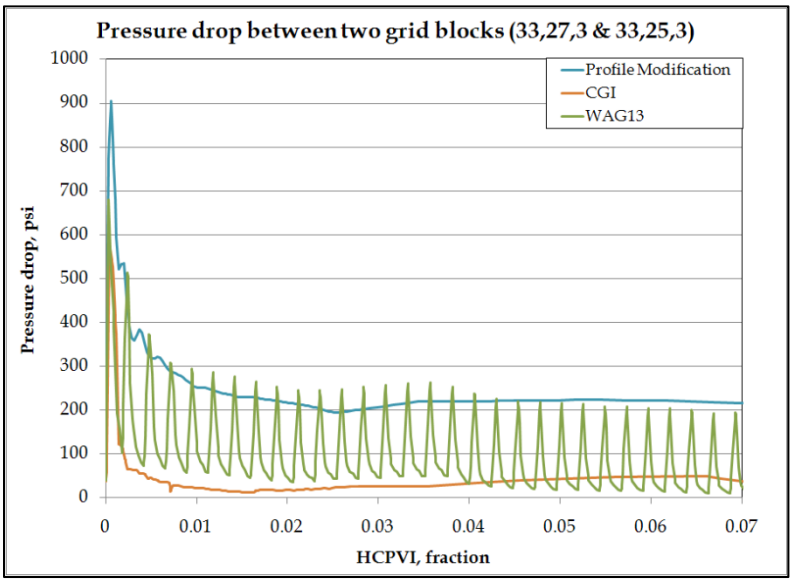

Figure 4.21: Pressure difference between the bottom hole pressure in the injector and a nearby grid block in the reservoir. This shows a gradually increasing pressure drop as we move from CGI to WAG to profile modification.

Table 4.6: Approximate gas breakthrough time for each recovery method.

Method	HCPVI, %
CGI	1.4
WAG 3:1	8
WAG 1:1	7.5
WAG 1:3	2.2
WAG 1:5	1.9
Profile Modification	2.8

4.4.4 CO_2 Utilization Rates

Gross CO_2 utilization rate is defined as the ratio of the cumulative amount of CO_2 injected to the cumulative oil produced (Taber, et al., 1997). This utilization rate is expected

to go down with the usage of WAG processes due to the lower volumes of CO_2 injected. Net CO_2 utilization is defined as the ratio of the amount of injected CO_2 trapped in the reservoir to the cumulative oil produced. Figure 4.22 shows the net CO_2 utilization rates of the three methods. A WAG ratio of 1:1 is shown in this graph since it is the WAG ratio which gives the highest oil recovery.

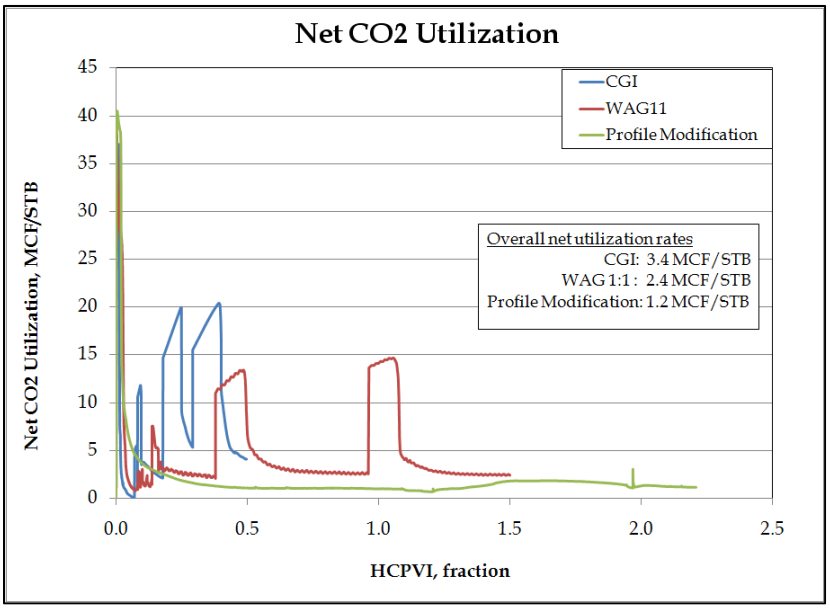

Figure 4.22: Net CO_2 Utilization of the three methods. Net CO_2 utilization decreases as we move from CGI to WAG 1:1 to profile modification.

Net utilization rates decrease for different methods with the highest utilization rate for CGI, and the least for profile modification. Hence, CGI requires more CO_2 to recover a barrel of oil and this is largely due to the inefficient sweep and cycling of injected CO_2 caused by the high permeability in layer 3. Profile modification greatly decreases the usage of CO_2 as it

contacts a larger volume of reservoir rock (Figure 4.18) and recovers more oil. In the case of WAG, the injected water, apart from providing better displacement is also trapped in reservoir rock which could have otherwise been occupied by CO_2. This leads to a lower CO_2 utilization.

4.4.5 Layer Injection Rates

Rate of injection into each of the 5 layers was plotted to understand which of the methods provides better conformance control. Figure 4.4, Figure 4.23 and Figure 4.16 show the injection rates into each layer for CGI, WAG and profile modification methods. The rates shown in Figure 4.23 correspond to the CO_2 injection cycle. Also, the presence of a blocking agent in layer 3 restricts gas entry into that layer thereby enabling gas to enter the reservoir through the remaining layers. This is one of the reasons vertical sweep increases in this method.

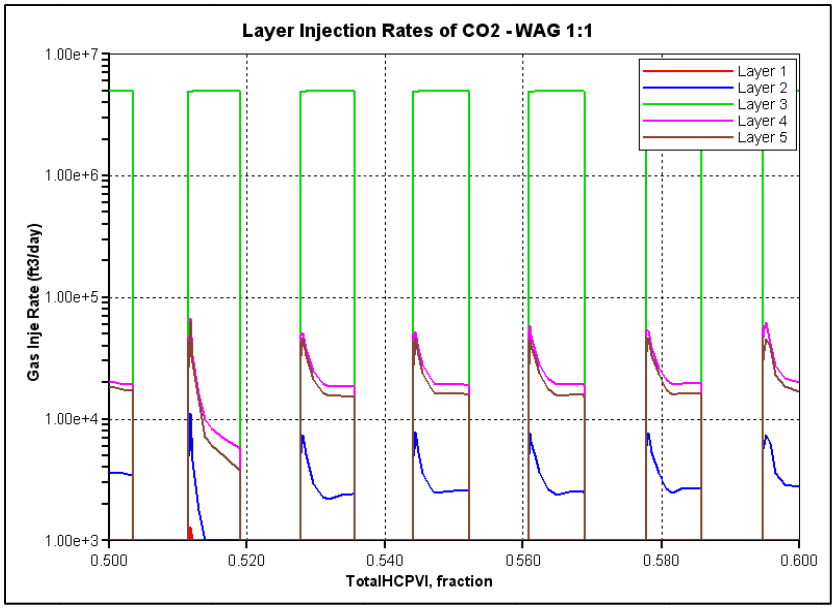

Figure 4.23: CO_2 Injection rates into all 5 layers during WAG 1:1 flood. In comparison with continuous CO_2 injection, the CO_2 injection rates into layers 1, 2, 4, and 5 have increased.

5 CONCLUSIONS AND DISCUSSION

This chapter summarizes the conclusions which were derived from the methods adopted for enhanced oil recovery in a heterogeneous formation. This section emphasizes the importance and applicability of WAG and profile modification as EOR methods for heterogeneous reservoirs. Additionally, the chapter also mentions some important discussions stemming from this thesis.

5.1 Conclusions

Profile modification greatly improves the vertical sweep efficiency in a highly heterogeneous heavy oil reservoir. The simulation models studied in this work were the ones in which the placement of blocking agent was mimicked by changing the relative permeability curves. In field operations, injection of a blocking agent like foam to the distances considered in this work would be difficult because of decreased injectivity.

An optimum WAG ratio of 1:1 was observed to result in highest recovery during both slim tube simulation studies and in field simulations. Along with improved recoveries, WAG improved CO_2 injection rates into layers which had low permeabilities. This is lower than the WAG ratio of 1:2 which yields highest recoveries in light oil reservoirs.

Mechanisms for oil recovery in these processes are similar (alteration of mobility) but the extent of the reduction in mobility differs between processes. Viscosity reduction in the oil

once it has been contacted by CO_2 was observed in each of the methods discussed. The fluid driving the reduced viscosity oil defines the mobility ratio. These values are around 15 for CGI and 8 for the WAG process. For the profile modification method, mobility ratio in the reservoir injected by the blocking agent is lower than CGI, whereas the mobility ratio in the rest of the reservoir is the same as for CGI process. The increased recovery from profile modification is controlled by the volume contacted by blocking agent. Mechanisms leading to better recovery then are decreases in oil viscosity, decreases in mobility ratio, and increases in rock volume contacted by blocking agent.

5.2 Discussion

Profile modification can be attained by placing gels, polymers or foam. The case discussed in section 4.3 relates to the usage of foam as a profile modification agent which decreases the gas relative permeability. The relative permeability depends on foam quality, temperature, rock properties, and several other properties. However, since GEM® was not built to model foam properties, the results obtained here could vary when the process is simulated using a numerical simulator capable of modeling foam properties. The gas relative permeabilities tables used in this case are constant for the entire duration of flood. In reality, the relative permeabilities also vary with time, foam quality, and several other parameters. With time, foam quality may degrade thereby increasing the gas relative permeability, rendering the process similar to a CO_2 flooding process.

As noted in chapter 4, the CO_2 front moves to the next producer well as the previous producer wells are shut in due to high GOR. Instead of shutting in the producer wells completely, choking back wells which have high GOR values may divert the CO_2 to areas that remain unswept. We expect that this would increase recovery rates and reduce the recycling of CO_2 but also increase the pressure in the reservoir.

Another way to recover more oil might be to drill infill wells. Simulations show the southwest section of the field is not being swept by any of the injected fluid. Drilling an infill well in the southwest section might result in better sweep in that part of the field.

5.3 Future Work

This work focuses on two of the alternatives to a CO_2 flood which could be applied in a field. In continuation with this work, future work must look into several other non-thermal EOR methods which could improve sweep in heavy oil reservoirs. These include, but are not limited to polymer flooding, foam assisted water alternating gas (FAWAG), and foam flooding. Understanding the mechanisms by which each of these methods contacts more rock and recovers oil would give insights into improving vertical sweep.

Huff-n-Puff methods and the effect of soak periods were not investigated in the current study. Gravity was found to be the reason oil was recovered from layer 2, and introducing a soak period could lead to gravity forces allowing more oil to be drawn into layer 3 where it can be produced.

A laboratory model similar to the one discussed in this work, a highly heterogeneous 5 layer model, could be built to investigate and verify some of the key observations made in this study. Important among these are the gravity effects to drain oil into the high permeability zone, the impact of a soak period on the extent of oil drained and recovered, and the effect of blocking agents in changing gas relative permeability and the stability of the blocking agent over a time.

Similar studies conducted on other heavy oil fields with heterogeneity problems can bring forth a better understanding of the processes which can improve sweep and those which do not. The methodology described and the steps followed in this thesis can act as a starting point for such studies.

REFERENCES

Ali, F. S. (1976). Non-Thermal Heavy Oil Recovery Methods. *Paper SPE 5983 presented at Rocky Mountain Regional Meeting of SPE.* Casper, 11-12 May: Society of Petroleum Engineers.

Bernard, G. G., and Holm, L. W. (1964). Effect of Foam on Permeability of Porous Media to Gas. *SPE Journal , Vol. 4* (Issue 3), 267-274.

Coats, K. H. (1980). An Equation of State Compositional Model. *SPE Journal , Vol. 20* (Issue 5), 363-376.

Computer Modeling Group Ltd. (2009). Calgary: CMG.

Computer Modeling Group. (2011). Personal Communication.

Craig, F. F. (1993). The Reservoir Engineering Aspects of Water Flooding. Dallas: SPE.

Di Julio, S. S., and Emanuel, A. S. (1989). Laboratory Study of Foaming Surfactant for CO2 Mobility Control. *SPE Reservoir Engineering , Vol. 4* (Issue 2), 136-142.

DOE. (2007, June 18). *Fact Sheet: U.S. Heavy Oil Resource Potential.* Retrieved October 18, 2009, from http://fossil.energy.gov: http://fossil.energy.gov/programs/reserves/npr/Heavy_Oil_Fact_Sheet.pdf

Dyer, S. B., and Ali, S. M. (1989). The potential of the Immiscible Carbon Dioxide Flooding Process for the Recovery of Heavy Oil. *Paper PETSOC SS 89 - 27 presented at the Petroleum Conference of the South Saskatchewan Section.* Regina, 25-27 September.

EIA. (March 2009). *Annual Energy Outlook 2009.* Energy Information Administration.

EOR Field Case Histories (SPE Reprint Series # 23). (1987). Richardson, Texas, USA: SPE.

Green, D. W., and Willhite, G. P. (1998). *Enhanced Oil Recovery* (Vol. 6). Rishardson, TX: Society of Petroleum Engineers.

Gunter, G. W., Finneran, J. M., Hartmann, D. J., and Miller, J. D. (1997). Early Determination of Reservoir Flow Units Using an Integrated Petrophysical Method. *Paper SPE 38679 MS presented at the SPE Annual Technical Conference.* San Antonio, .

Hatzignatiou, D. G., and Lu, Y. (1994). Feasibility study of CO2 Immiscible Displacement Process in Heavy Oil Reservoirs. *Paper PETSOC 94-90 presented at the 45th Annual Technical Meeting.* Calgary, 12-15 June: Petroleum Society of CIM.

Holm, L. W. (1968). The Mechanism of Gas and Liquid Flow Through Porous Media in the Presence of Foam. *SPE Journal , Vol. 8* (Issue 4), 359-369.

Holm, L. W., and Garrison, W. H. (1988). CO2 diversion with Foam in an Immiscible CO2 Field Project. *SPERE , Vol. 3* (Issue 1), 112-118.

Hong, K. C. (1982). Lumped-Component Characterization of Crude Oils for Compositional Simulation. *Paper SPE 10691 presented at the SPE Enhanced Oil Recovery Symposium.* Tulsa, 4-7 April: SPE.

Jarrell, P. M., Fox, C. E., Stein, M. H., and Webb, S. L. (2002). Practical Aspects of CO2 Flooding. Richardson: SPE.

Jha, K. N. (1986). A Laboratory Study of Heavy Oil Recovery with Carbon Dioxide. *Journal of Canadian Petroleum Technology , Vol. 25* (Issue 2), 54-63.

Klins, M. A., and Ali, F. S. (1982). Heavy Oil Production by Carbon Dioxide Injection. *Journal of Canadian Petroleum Tecchnology , Vol. 21* (Issue 5), 64-72.

Lake, L. W. (1989). *Enhanced Oil Recovery.* New Jersey: Prentice Hall.

Li, D., Kumar, K., and Mohanty, K. K. (2003). Compositional Simulation of WAG Processes for a Viscous Oil. *Paper 84074 presented at Annual Technical Conference and Exhibition.* Denver, 5 - 8 October.

Llave, F., Chung, F. T.-H., Louvier, R. W., and Hudgins, D. A. (1990). Foams as Mobility Control Agents for Oil Recovery by Gas Displacement. *Paper SPE 20245-MS presented at the Enhanced Oil Recovery Symposium.* Tulsa, 22-25 April.

Lovy, D. (1996). WINDIG. *Version 2.5* .

Mangalsingh, D., and Jagai, T. (1996). A laboratory Investigation of the Carbon Dioxide Immiscible Process. *Paper SPE 36134-MS presented at the SPE Latin American/Carribean Petroleum Engineering Conference.* Port-of-Spain, 23-26 April.

Martin, F. D., Kovarik, F. S., Chang, P. W., Goldman, I. M., and Philips, J. C. (1988). Gels in CO2 Profile Modification. *Paper SPE 17330-MS presented at the SPE Enhanced Oil Recovery Symposium.* Tulsa, 16-21 April: SPE.

McMullan, J. (2001). Retrieved July 3, 2009, from http://www.enrg.lsu.edu/node/308

Moffitt, P. D., and Zornes, D. R. (1992). Postmortem Analysis: Lick Creek Meakin Sand Unit Immiscible CO2 Waterflood Project. *Paper SPE 24933-MS presented at the SPE Annual Technical Conference and Exhibition.* Washington DC, 4-7 October: Society of Petroleum Engineers.

Mungan, N. (1981). Carbon dioxide flooding - fundamentals. *Journal of Canadian Petroleum Technology , Vol. 20* (Issue 1), 87-92.

Nagineni, V. R., D'Souza, D., Holden, C., and Hughes, R. G. (2011). Using Core Data to Study and Optimize the Completion Strategy in EOR Operations. *Paper SPE 145106 to be presented at the SPE EOR Conference.* Kuala Lumpur.

Pedersen, K. S., Fredenslund, A., Christensen, P. L., and Thomassen, P. (1984). Viscosity of Crude Oils. *Chemical Engineering Science , Vol. 39* (Issue 6), 1011-1016.

Reid, T. B., and Robinson, H. J. (1981). Lick Creek Meakin Sand Unit Immiscible CO2/Waterflood Project. *Journal of Petroleum Technology , Vol. 33* (Issue 9), 1723-1729.

Rojas, G. A., and Farouq Ali, S. M. (1988). Dynamics of Subcritical CO2/Brine Floods for Heavy-Oil Recovery. *SPE Reservoir Engineering , Vol. 3* (Issue 1).

Rojas, G., and Farouq Ali, S. M. (1986). Scaled model studies of carbon dioxide/brine injection strategies for heavy oil recovery from thin formations. *Journal of Canadian Petroleum Technology , Vol. 25* (Issue 1), 85-94.

Senocak, D. (2008). *Evaluation of Sweep Efficiency of a mature CO2 Flood in Little Creek Field, Mississippi.* Louisiana State University, MS Thesis, Craft and hawkins Department of Petroleum Engineering, Baton Rouge.

Spivak, A., and Chima, C. M. (1984). Mechanisms of Immiscible CO2 Injection in Heavy Oil Reservoirs, Wilmington Field, CA. *Paper SPE 12667-MS presented at the SPE Enhanced Oil Recovery Symposium.* Tulsa, 15-18 April.

Surguchev, L. M., Korbol, R., Haugen, S., and Krakstad, O. S. (1992). Screening of WAG Injection Strategies for Heterogeneous Reservoirs. *Paper SPE 25075-MS presented at the European Petroleum Conference.* Cannes, France, 16-18 November: SPE.

Syahputra, A. E., Tsau, J.-S., and Grigg, R. B. (2000). Laboratory Evaluation of Using Lignosulfonate and Surfactant Mixture in CO2 Flooding. *Paper SPE 59368-MS presented at the SPE/DOE Improved Oil Recovery Symposium.* Tulsa, 3-5 April.

Taber, J. J., Martin, F. D., and Seright, R. S. (1997). EOR Screening Criteria Revisited - Part 2: Applications and Impact of Oil Prices. *SPE Reservoir Engineering , Vol. 12* (Issue 3), 199-206.

Worldwide EOR Survey, Drilling/Producion Special Report. (2006). *Oil and Gas Journal* , 15-18.

Ye, Z., Pu, W., Zhang, S., and Chen, T. (1997). Laboratory Study on Profile Modification by Using Foamed Polymer Solution. *Paper PETSOC 97-128 presented at the Annual Technical Meeting of The Petroleum Society of Canada.* Calgary, 8-11 June.

Zhang, Y. P., Sayegh, S., and Huang, S. (2006). Enhanced Heavy Oil Recovery by Immiscible WAG Injection. *Paper PETSOC 2006-014 presented at the Canadian International Petroleum Conference.* Calgary, 13-15 June.

APPENDIX A

In chapter 2, the fluid characterization of the reservoir crude was discussed in detail. The following plots show the match of results of CCE experiments conducted in laboratory and the ones conducted using CMG-WINPROP®. These experiments are conducted at three different mole fraction concentrations of CO_2 – 0%, 20% and 35%.

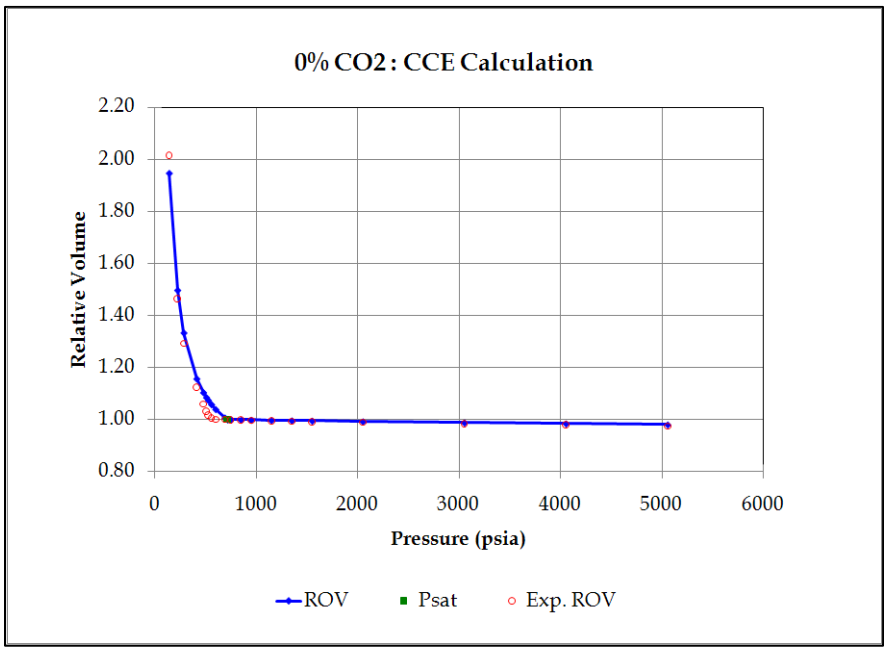

Figure A-1: CCE data match of Relative Volume of oil in comparison with its volume at bubble point (CO_2 mole fraction = 0%)

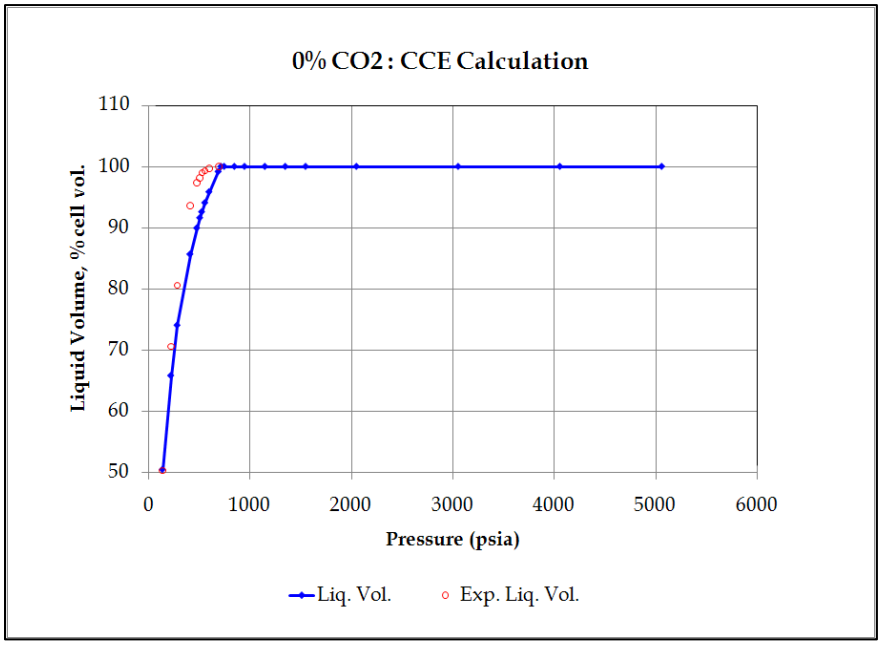

Figure A-2: CCE data match of volume of liquid in crude oil considering the volume at bubble point as 100% (CO_2 mole fraction = 0%)

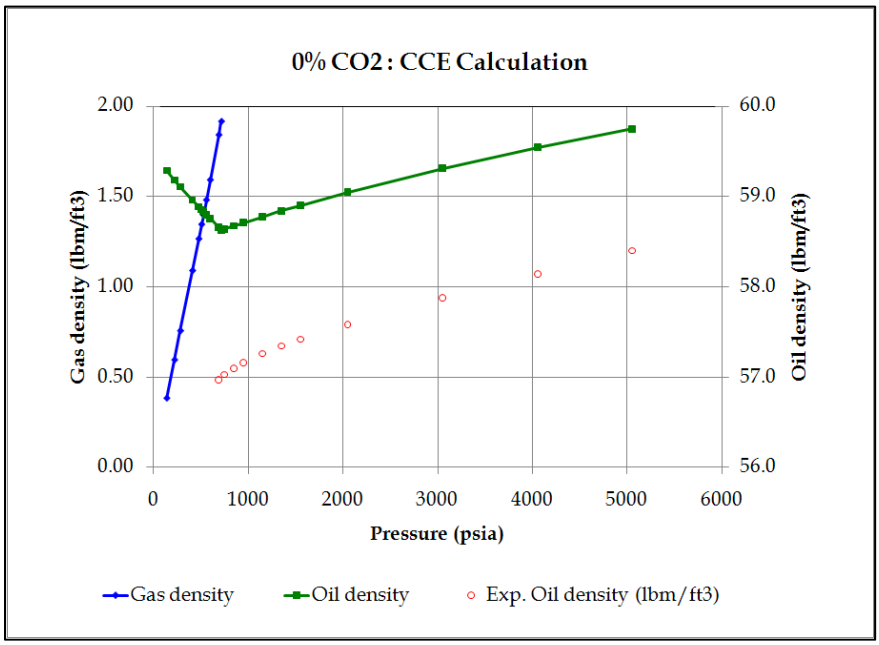

Figure A-3: CCE data match of oil densities (CO_2 mole fraction = 0%)

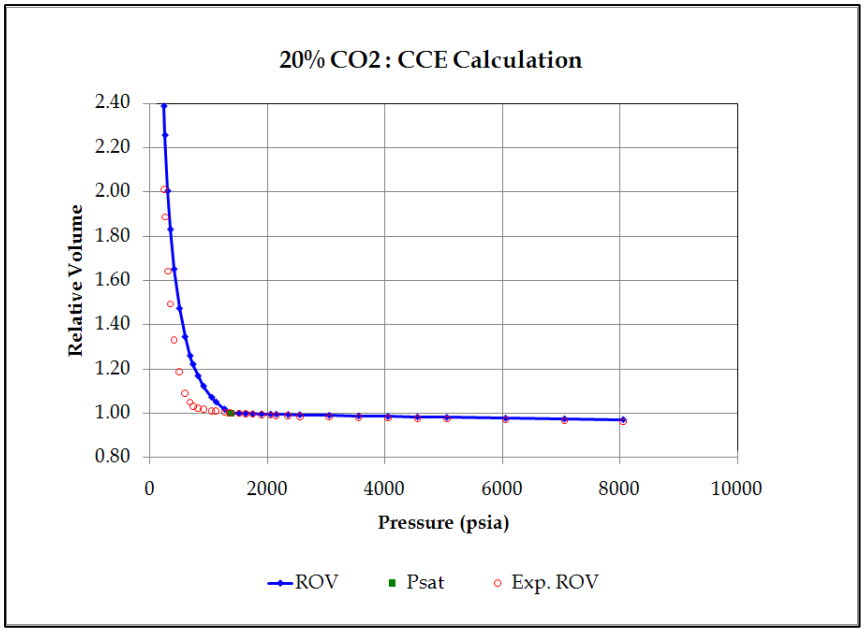

Figure A-4: CCE data match of Relative Volume of oil in comparison with its volume at bubble point (CO_2 mole fraction = 20%)

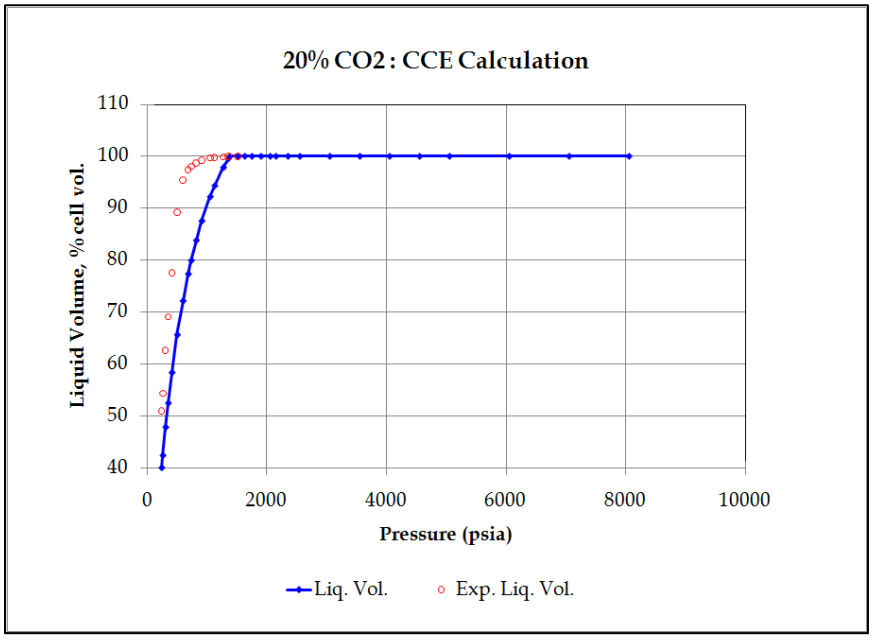

Figure A-5: CCE data match of volume of liquid in crude oil considering the volume at bubble point as 100% (CO_2 mole fraction = 20%)

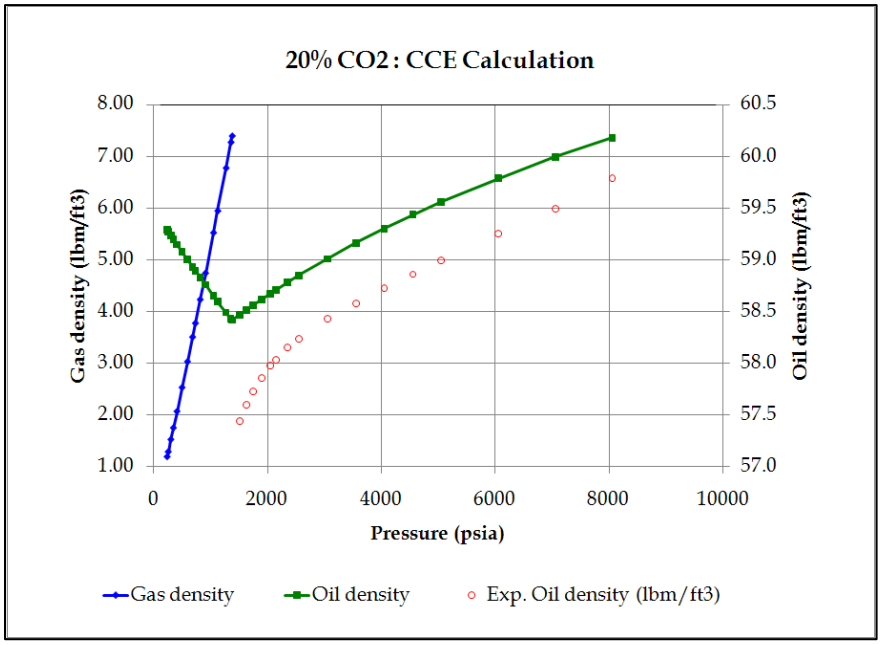

Figure A-6: CCE data match of oil densities (CO_2 mole fraction = 20%)

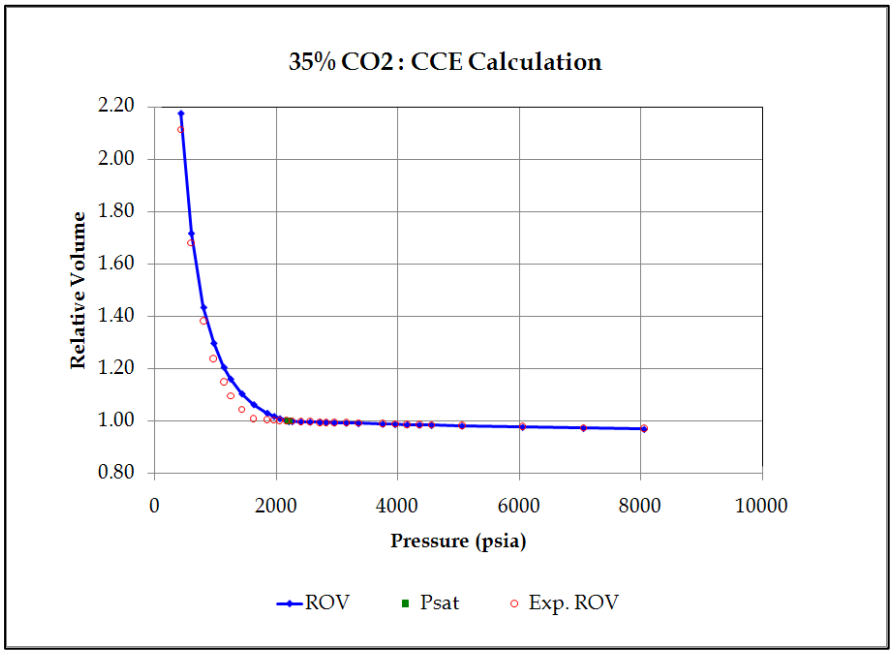

Figure A-7: CCE data match of Relative Volume of oil in comparison with its volume at bubble point (CO_2 mole fraction = 35%)

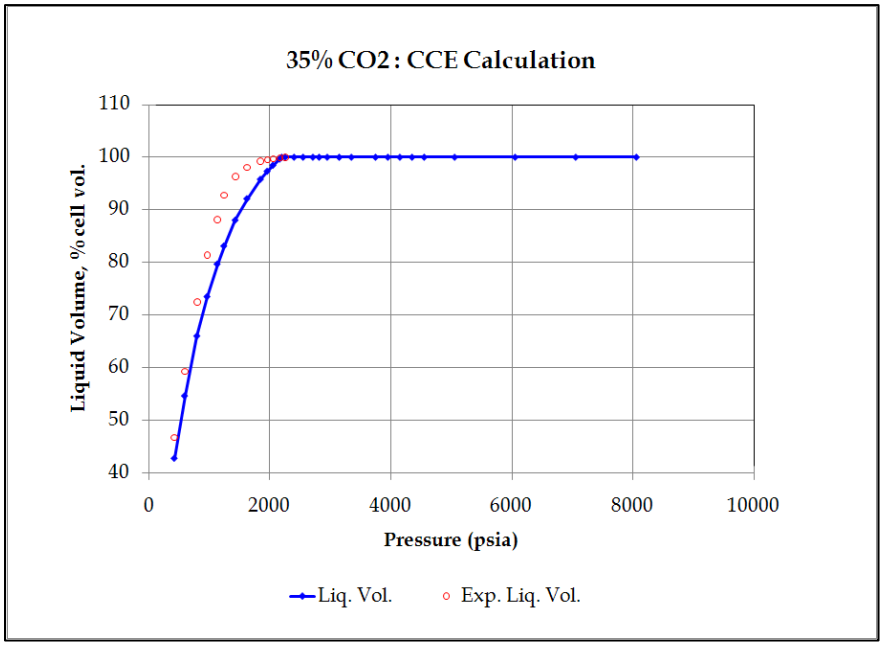

Figure A-8: CCE data match of volume of liquid in crude oil considering the volume at bubble point as 100% (CO_2 mole fraction = 35%)

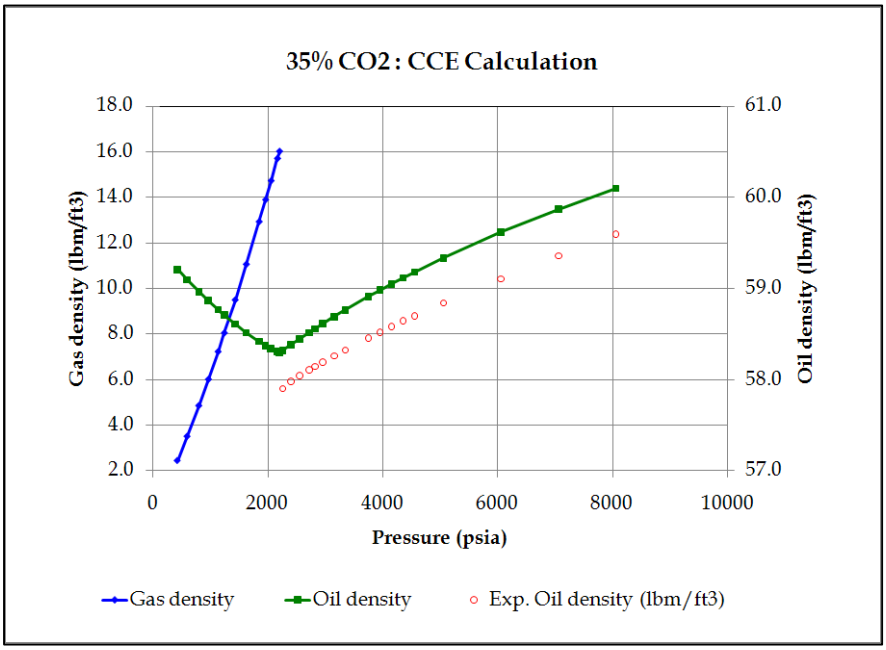

Figure A-9: CCE data match of oil densities (CO_2 mole fraction = 35%)

APPENDIX B

In chapter 2, the construction of reservoir model and its subsequent history match is discussed in detail. The following plots show the results of history matching for individual wells.

History Match Plots

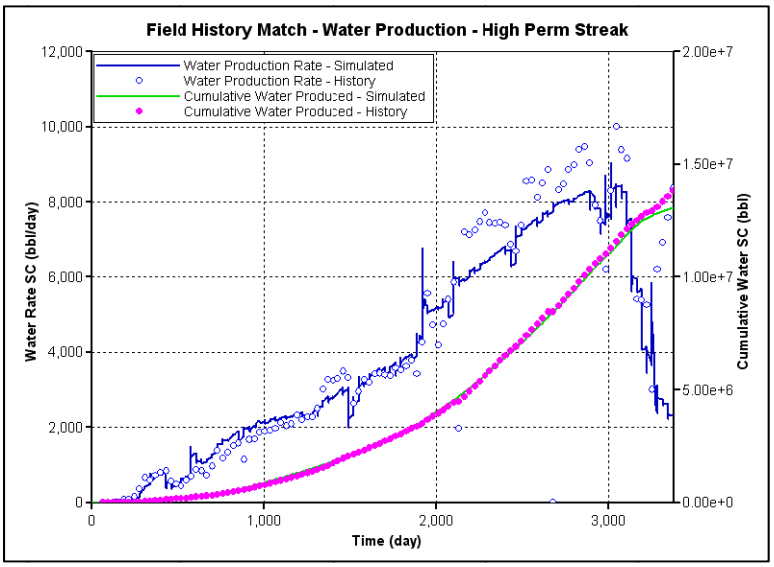

Figure B-1: Field history match of water production from the reservoir using a high permeability streak of 1 Darcy.

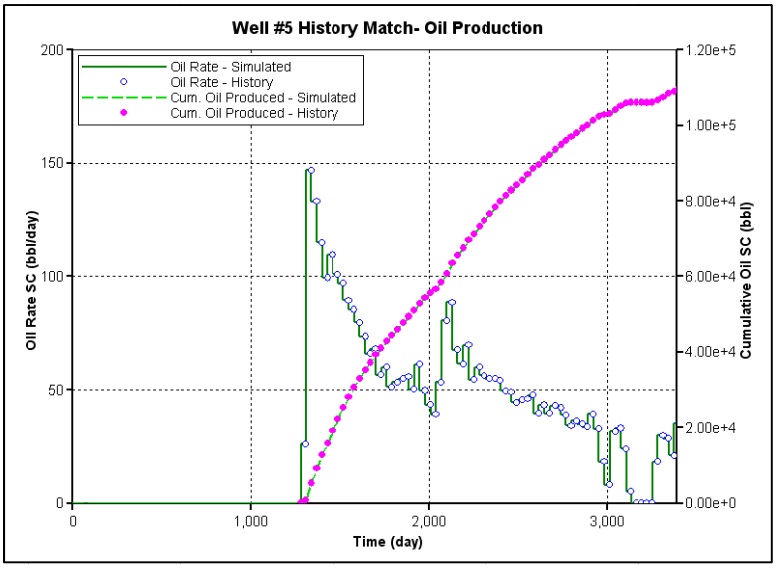

Figure B-2: Oil production history match of Well #5.

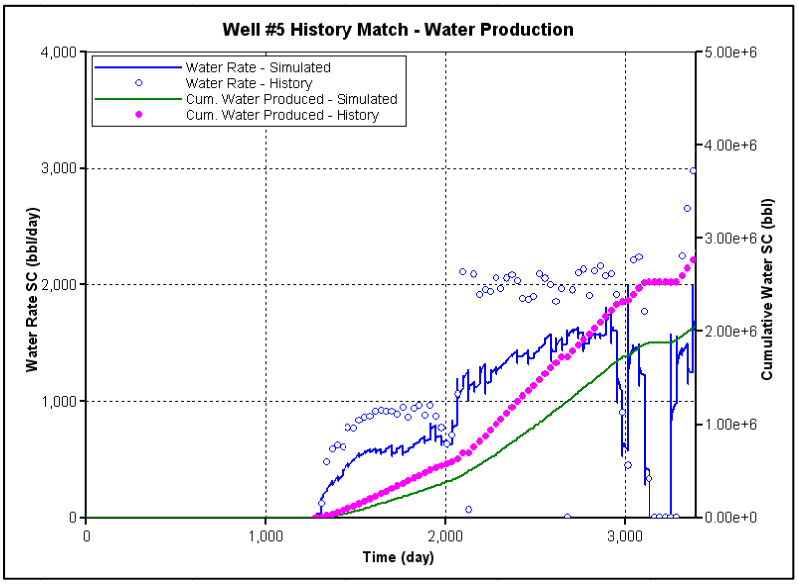

Figure B-3: Water production history match of Well #5.

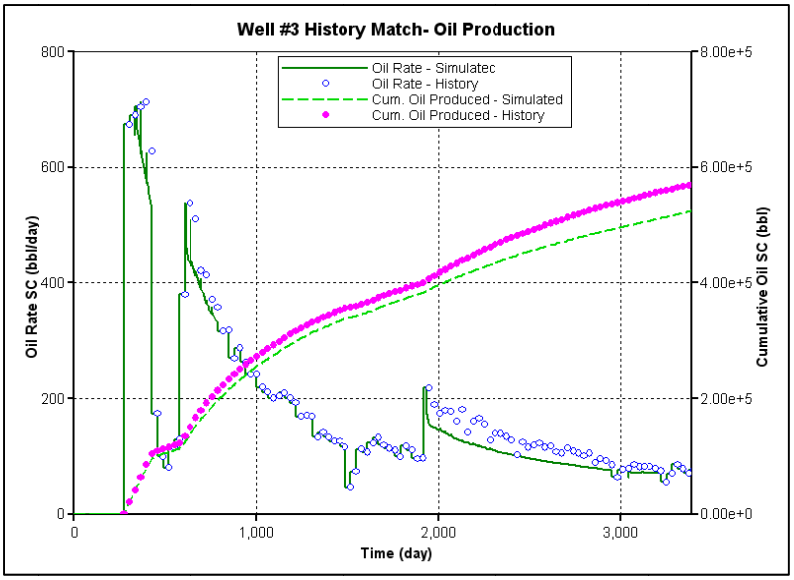

Figure B-4: Oil production history match of Well #3.

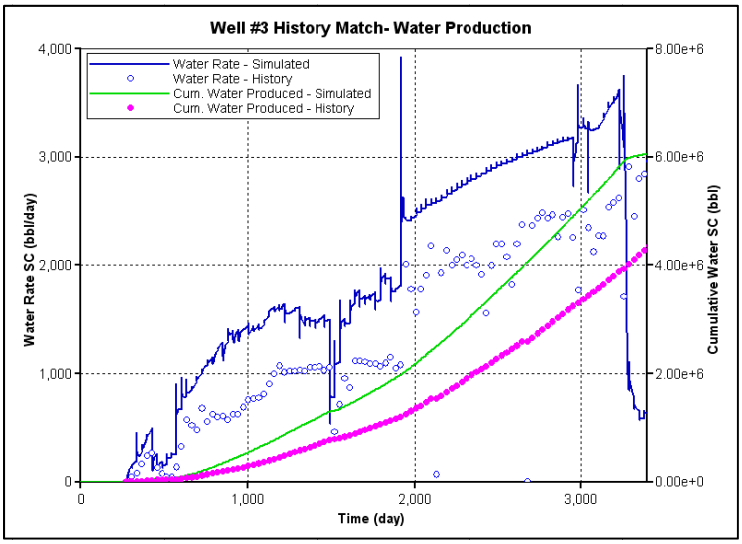

Figure B-5: Water production history match of Well #3.

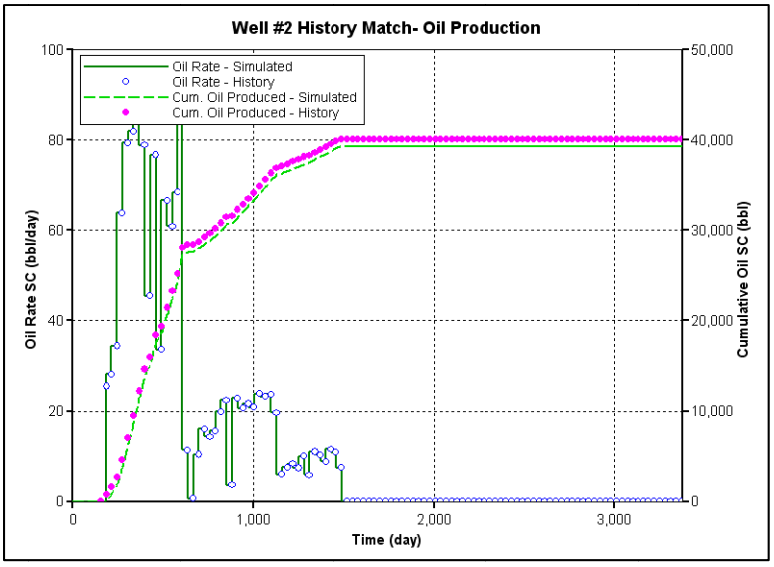

Figure B-6: Oil production history match of Well #2.

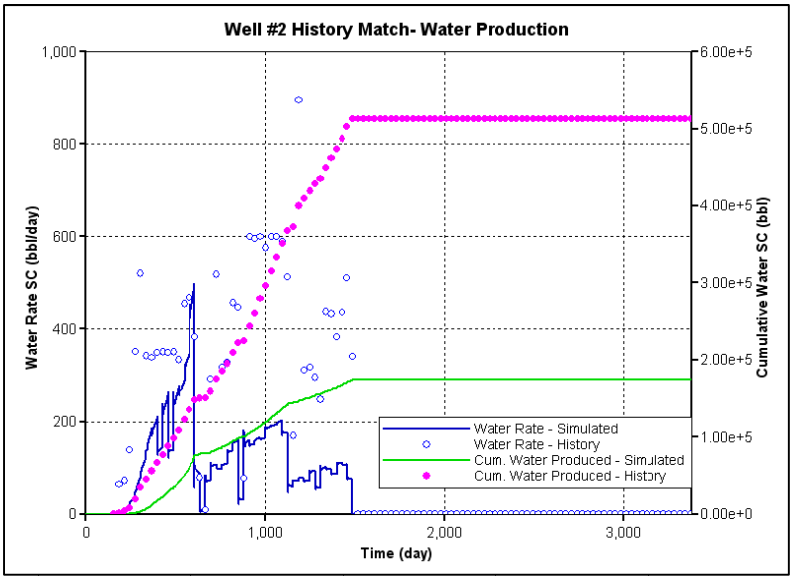

Figure B-7: Water production history match of Well #2.

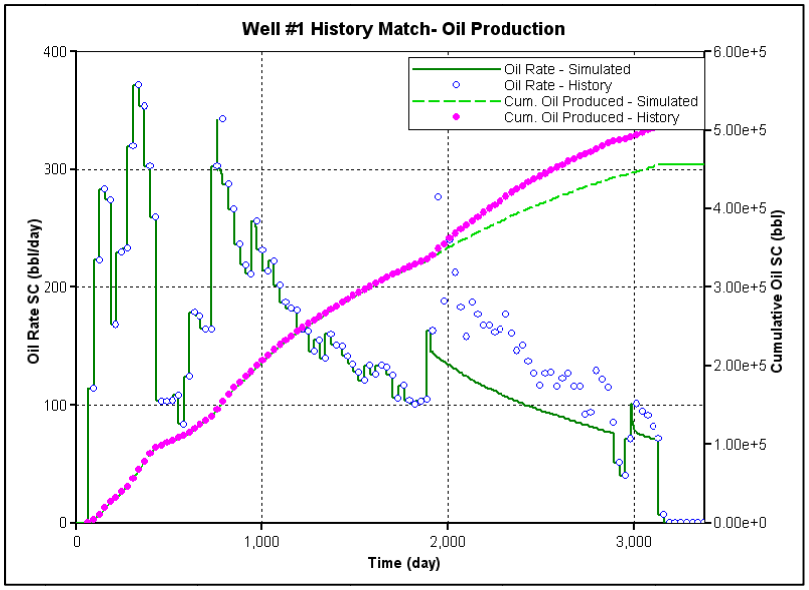

Figure B-8: Oil production history match of Well #1.

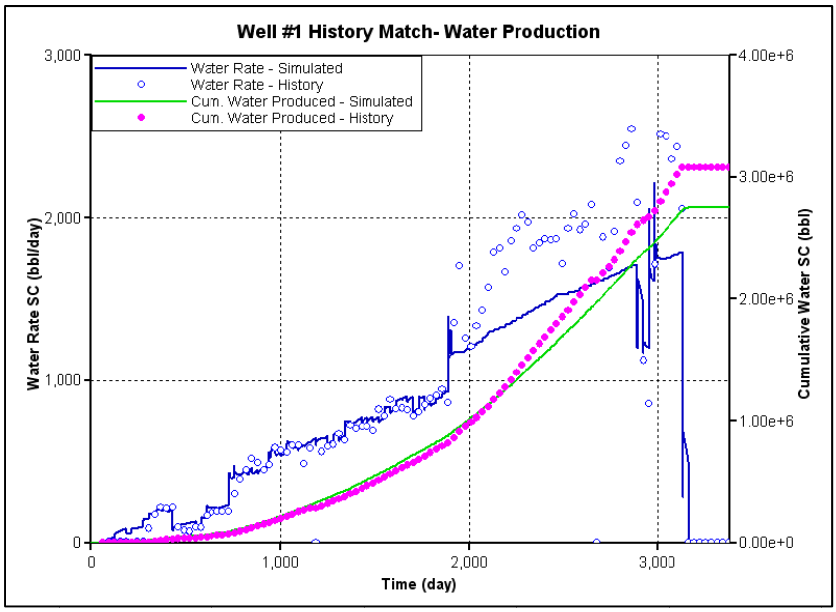

Figure B-9: Water production history match of Well #1.

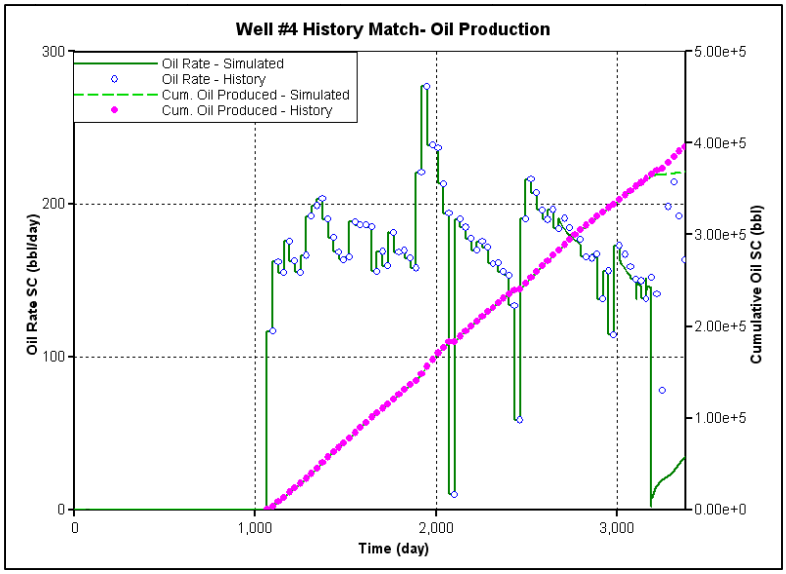

Figure B-10: Oil production history match of Well #4.

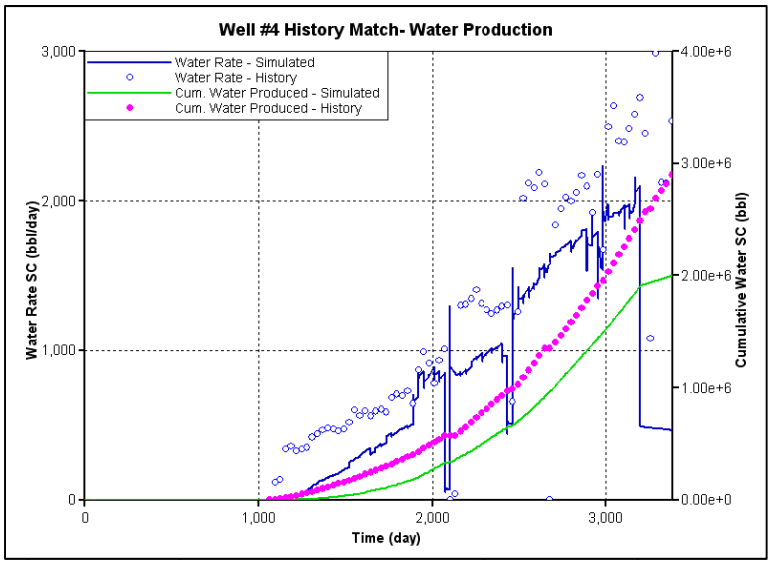

Figure B-11: Water production history match of Well #4.

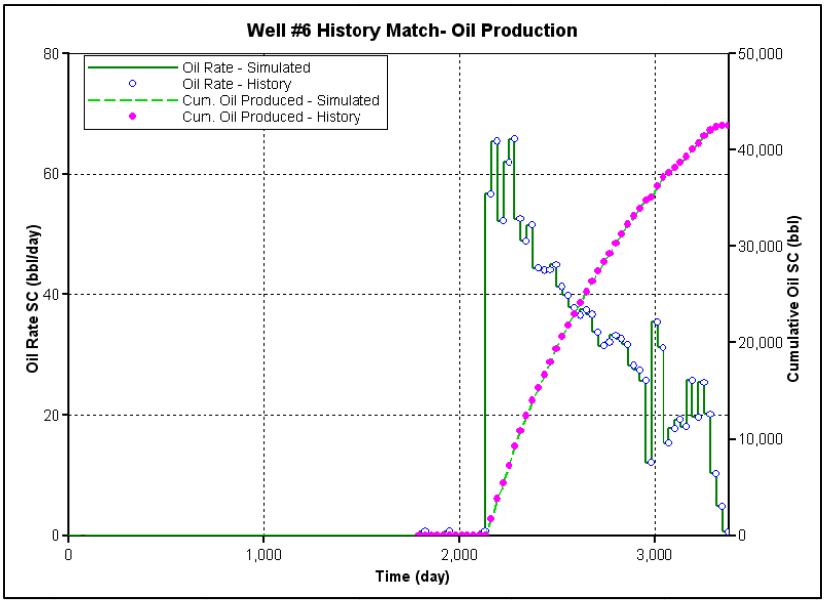

Figure B-12: Oil production history match of Well #6.

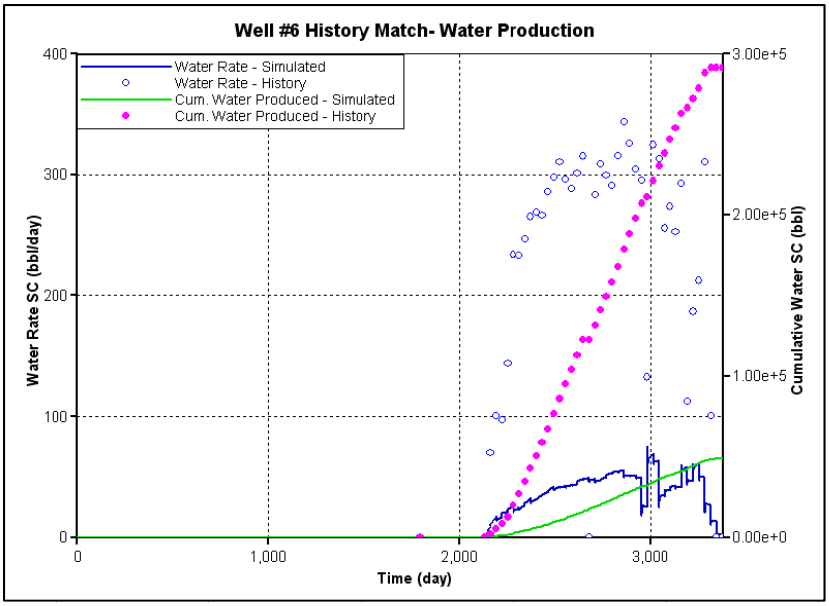

Figure B-13: Water production history match of Well #6.

Relative Permeability Plots

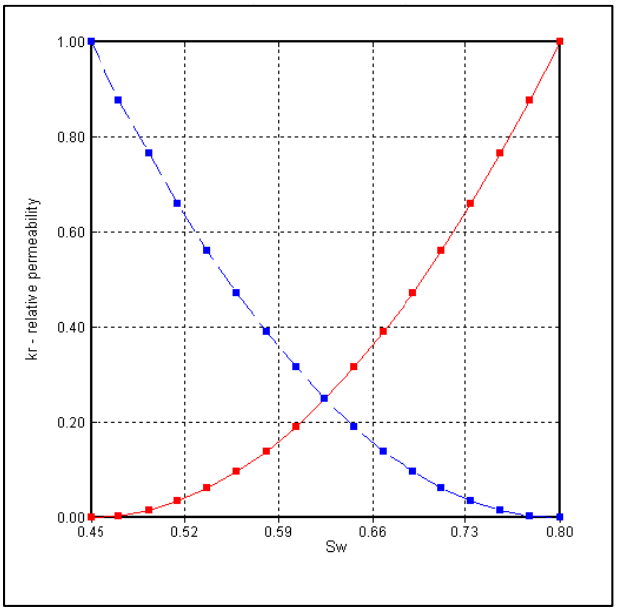

Figure B-14: Initial oil-water relative permeability curve.

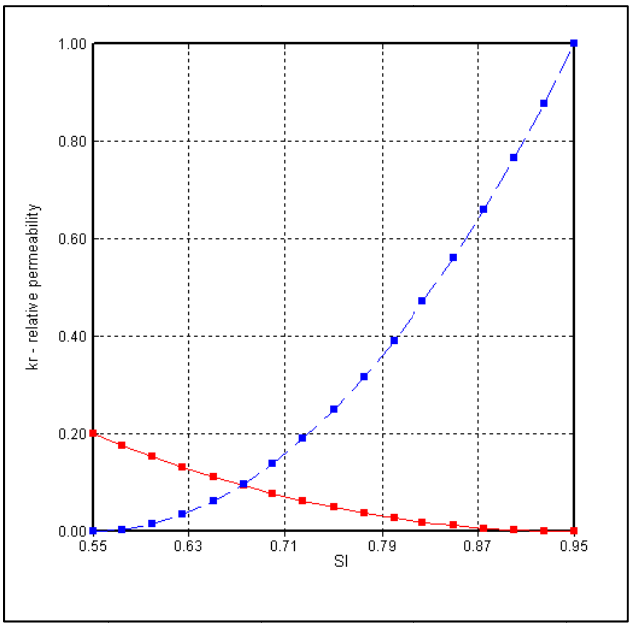

Figure B-15: gas-liquid relative permeability curve after history matching and calibration for breakthrough time.

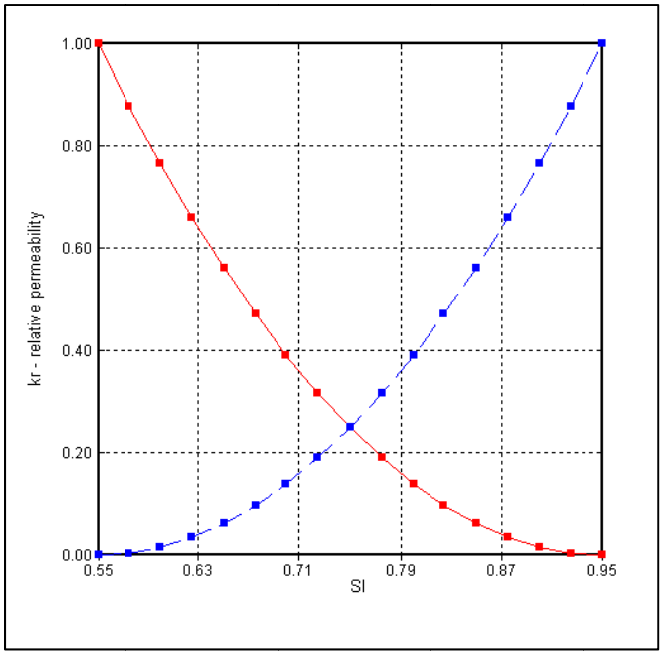

Figure B-16: Initial gas-liquid relative permeability curve

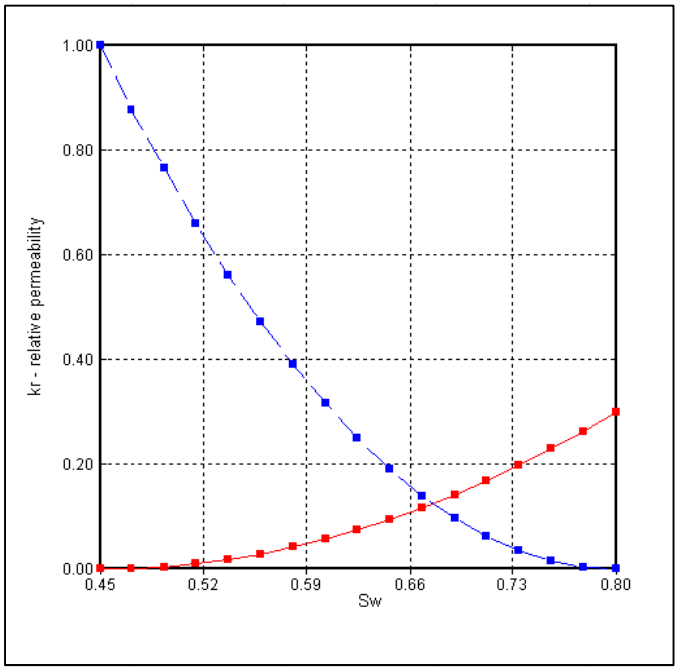

Figure B-17: Oil-water relative permeability curve after history matching and calibrating for CO_2 breakthrough time.

VITA

Venu Gopal Rao Nagineni was born in Andhra Pradesh, India, in 1984. After completing his high school education in Hyderabad, India, he obtained a bachelor's degree in petroleum engineering from Indian School of Mines, Dhanbad, India, in 2006. He worked in the oil and gas software consulting industry for one and a half year and later joined the Craft and Hawkins Department of Petroleum Engineering at Louisiana State University in 2008. He received a Master of Science in Petroleum Engineering in the spring of 2011.